

COULOMB EXCITATION OF ^{140}Sm

by

Trond Wiggo Johansen

THESIS

for the degree of

MASTER OF SCIENCE



Faculty of Mathematics and Natural Sciences
University of Oslo

September 2019

Abstract

To my family, for all their support and encouragement!

Acknowledgements

Supervisors Andreas Görzen and Katarzyna Hadyńska-Klęk
Nuclear Physics Group
Computational Physics Group, Morten Hjorth-Jensen
CERN-ISOLDE, Liam Gaffney
Lillefy, FFU, Fysikkforeningen
My family
Morten, Alex and Astrid.
Ina, for pushing me towards excellence, I love you.

Collaboration details

ENSAR2: European Nuclear Science and Applications Research - 2 <http://www.ensarfp7.eu>, UiO, ISOLDE, other contributors to the experiment?

Trond Wiggo Johansen

September, 2019



Contents

1	Introduction	11
2	Theory	13
2.1	Oppgaveteksten (skal fjernes!)	15
3	Coulomb excitation experiment	17
3.1	ISOLDE at CERN	18
3.1.1	Beam production	18
3.1.2	Target	21
3.2	Miniball spectrometer	21
3.2.1	Target chamber	21
3.2.2	Particle detector, DSSSD (CD)	22
3.2.3	γ detectors, high-purity germanium (HPGe)	22
3.3	Experimental setup	23
3.4	Data acquisition system	24
4	Data analysis	33
4.1	Data and sorting	38
4.1.1	Digital electronics - unnecessary?	38
4.1.2	???	40
4.2	Helping scripts	40
4.3	Simulation	41
4.4	Calibration	43
4.4.1	Particle detector	48
4.4.2	Gamma detectors	49
4.5	Doppler correction	49
5	Experimental results	55
6	Discussion	57
7	Summary and outlook	59
Appendices		61
Appendix A	Symbol list	63
Appendix B	Acronyms and abbreviations	65
Appendix C	Two-particle collision	67
C.1	Laboratory (LAB) frame of reference	67

C.2 Center of mass (CM) frame of reference	70
C.3 Connection between the LAB frame and the CM frame	72
Appendix D Source code	77
Appendix E Connecting MiniballCoulexSort with ROOT	79
Appendix F Running ROOT and MiniballCoulexSort from anywhere in the terminal	81
Appendix G Other appendices	83
Bibliography	85

Chapter 1

Introduction

+ Motivation

The experiment has been done before, with lower energy (and another target), Malin Klintefjord. <http://urn.nb.no/URN:NBN:no-56121>

Malin Klintefjord PhD thesis [1] with the three papers [2], [3] and [4] on ^{140}Sm .

Experiment conducted 8th - 14th of August 2017.

Tilbakemelding:

old REX-ISOLDE post-accelerator limited to 2.8 MeV/u (low Coulomb excitation cross section, low probability for multi-step excitation). Mo target was chosen to maximize cross section at this energy, and to normalize $B(E2; 0^+ \rightarrow 2^+)$ value in ^{140}Sm to the well-known $B(E2)$ value for the target.

New HIE-ISOLDE: energies up to 10 MeV/u \implies we can choose high-Z target (Pb) \implies high Coulex cross section, especially for multi-step. Also: $B(E2)$ for ^{140}Sm now known from previous experiment (and a lifetime measurement) \implies no need for normalization: we can use the known $B(E2; 0^+ \rightarrow 2^+)$ to normalize the transition probabilities for the higher-lying transitions. Chosen 4.7 MeV/u as the highest possible energy that is safe for Pb (distance of closest approach large enough to exclude nuclear interaction.)

Chapter 2

Theory

Table 2.1: Values of the fundamental physical constants from the National Institute of Standards and Technology (NIST) Physics Laboratory [5].

Quantity	Symbol	Numerical value	Unit
Speed of light in vacuum	c	299792458	m/s
Elementary charge	e	$1.602176634 \cdot 10^{-19}$	C
Electron volt	eV	$1.602176634 \cdot 10^{-19}$	J
Atomic mass unit	u	$1.66053906660(50) \cdot 10^{-27}$	kg

Isotope notation:



where X is the chemical symbol of the element, A is the nucleon number (mass number, $A = Z + N$), Z is the atomic number (proton number), N is the neutron number and Q is the charge ($Q = Z$ protons – i electrons).

Why CoulEx? https://iks32.fys.kuleuven.be/wiki/brix/images/5/58/10_20151123_Illana_BriX15_web.pdf

Magic numbers: 2, 8, 20, 28, 50, 82, 126

Maria Goeppert Mayer “discovered” them in ~1945. Observation of periodicity in binding energy \Rightarrow shell model for nuclei.

Eugene Wigner believed in liquid-drop model, did not trust new theory \Rightarrow called these numbers “magic”.

Source: https://ocw.mit.edu/courses/nuclear-engineering/22-02-introduction-to-applied-nuclear-physics/lecture-notes/MIT22_02S12_lec01.pdf

Quadrupole deformation of nuclei.

Shape coexistence possible for certain regions of N and Z .

- triaxial shape / shape coexistence
- benchmark for theoretical models
- transition probabilities and quadrupole moments between several excited states are not known
- fundamental research

COULEX:

- nucleus excited by electromagnetic interaction.
- de-excitation → gamma

Tilbakemelding:

shape coexistence often found near closed shells. Example: neutron deficient Hg nuclei ($Z = 80$ just below 82 shell closure, $N \sim 104$: neutron mid-shell).

^{140}Sm : $N = 78$, just below $N = 82$ shell closure, $Z = 62$: mid-shell.

Typical indication for shape coexistence: 0^+ states (often at low energy).

^{140}Sm was thought to have a low-lying 0^+ state [Firestone], but this state was shown to be 2^+ [Suoranczyk?]. Indication for 0^+ states around 1.5 MeV.

One of the objectives of this experiment: clarify the nature/structure of these 0^+ states.

Shape transition: Sm-144 ($Z = 62$, $N = 82$) spherical. Adding neutrons: transition of $N = 90$ from spherical to prolate deformed → shape-phase transition, so called X(5) critical-point symmetry.

Taking out neutrons: very neutron-deficient Sm nuclei are also prolate deformed (e.g. Sm-132), but for ^{140}Sm : indication for triaxiality/ γ -softness [Klintefjord] → another form of shape-phase transition/critical point behavior \implies E(5) [Iachello?]. ^{140}Sm could be one of the best examples for E(5) symmetry \implies need transition probabilities from higher-lying states to confirm.

Some suggestions:

- general things about nuclei shapes
- multipole expansion, shape parameters (5 parameters, 3 for space, 2 for deformation β , γ), ...
- quadrupole moments: intrinsic (body-fixed frame), spectroscopic (lab frame)
- transition probabilities, el.magn. matrix elements
- rotations and vibrations → energy spectra, $B(E2)$ values
- Casten triangle (spherical vibrator, deformed rotor, γ -soft + X(5), E(5)), expected spectrum for E(5) nuclei
- the basics of Coulomb excitation

NOTES TO BE REMOVED!!

2.1 Oppgaveteksten (skal fjernes!)

Oppgavens mål:

The ISOLDE facility at CERN has been upgraded to provide higher energies and intensities for radioactive ion beams. A new experiment to study ^{140}Sm was performed in the summer of 2017. The goal of the experiment was to measure electromagnetic transition probabilities and electric quadrupole moments for several excited states in ^{140}Sm by measuring Coulomb excitation probabilities. A large data set was obtained using silicon detectors to determine the energies and angles of scattered particles, and germanium detectors to measure gamma rays from excited states in ^{140}Sm .

The goal of the master thesis is to analyze the data from this experiment. The required tasks include development and improvement of data analysis software to determine Coulomb excitation yields. These yields will then, in a second step, be compared to theoretical calculations and transition probabilities and quadrupole moments will be extracted using chi-square minimization procedures.

Prosjektbeskrivelse (omfang 60 studiepoeng):

The shape of an atomic nucleus is determined by a delicate interplay between macroscopic (liquid drop) properties and microscopic shell effects. Nuclei with filled proton or neutron shells (i.e. magic nuclei) are generally spherical in shape, whereas nuclei with open shells gain energy by assuming a deformed shape. Depending on the occupation of specific orbitals, the nuclear shape can change drastically by adding or removing protons or neutrons. Certain nuclei exhibit shape coexistence, i.e. the coexistence of quantum states that correspond to different shapes. Because the shape of a nucleus is so sensitive to the underlying nuclear structure and to changes of the proton and neutron numbers, the excitation energy, or the angular momentum, observables related to the nuclear shape are used as benchmarks for theoretical models.

Nuclei in the rare earth region, and in particular the chain of samarium isotopes, exhibit a variety of shape effects. The Sm isotope with closed neutron

shell at N=82, ^{144}Sm , is spherical in shape. Adding neutrons to ^{144}Sm changes the deformation to an elongated (prolate) quadrupole shape. The transition from spherical to prolate shape, which occurs for ^{152}Sm at N=90, can be interpreted as a shape-phase transition. Flattened (oblate) quadrupole shapes are predicted by theory to occur below the N=82 shell closure. An earlier experiment studying ^{140}Sm at CERN-ISOLDE found triaxial shape for this isotope, i.e. a shape where all three principal axes of the ellipsoid have different lengths. ^{140}Sm can therefore be considered to lie at the critical point of a phase transition from spherical to deformed, and from prolate to oblate shape.

Foreløpig tittel:
Coulomb excitation of ^{140}Sm

Metoder som tenkes benyttet:
Multi-step Coulomb excitation with radioactive beam, isotope separation on-line technique, nuclear spectroscopy, particle-gamma and particle gamma-gamma coincidence analysis, advanced chi-square minimization procedures.

Sjekk sensorveiledning!!

Fjern blå linker in-text før innlevering!!

Chapter 3

Coulomb excitation experiment

Other info sources:

- ISOL & Post acceleration: https://www.euroschoolonexoticbeams.be/site/files/nlp/LNP700_contrib2.pdf
- ISOL RIB (2004): <http://accelconf.web.cern.ch/AccelConf/e04/PAPERS/TUXCH01.PDF>
- RIB (2017): <http://iopscience.iop.org/article/10.1088/1361-6471/aa990f/pdf>
- RIB: http://publications.lib.chalmers.se/records/fulltext/175494/local_175494.pdf
- RIB: <https://www.sciencedirect.com/science/article/pii/S0168583X02018864>
- Post-accelerated beams ISOLDE: <http://iopscience.iop.org/article/10.1088/1361-6471/aa78ca>
- PSB: <https://www.sciencedirect.com/science/article/pii/0168583X92959079>
- PSB: <https://home.cern/science/accelerators/proton-synchrotron-booster>
- RILIS ISOLDE: <https://www.sciencedirect.com/science/article/pii/S0168583X13008914>
- HIE-ISOLDE publications: <http://hie-isolde-project.web.cern.ch/hie-isolde-publications>
- Miniball pictures: <https://cds.cern.ch/record/844871?ln=en>
- The MINIBALL array [6]

3.1 ISOLDE at CERN

The acronym ISOLDE stands for Isotope Separator On Line DEvice. ISOLDE is a Radioactive Ion Beam (RIB) facility at CERN in Meyrin, Switzerland. [Figure 3.1](#) shows the CERN accelerator complex, where ISOLDE is located beside the Proton Synchrotron Booster (PSB). The facility can produce over 1000 different radionuclides to be used in a wide variety of experiments in nuclear physics, atomic physics, solid state physics, life sciences and fundamental interactions. Experiments have been performed at ISOLDE since 1967 and since 2001 experiments with post-accelerated RIBs have been conducted. The High Intensity and Energy upgrade (HIE-ISOLDE) have made it possible to deliver energies up to 10 MeV/u in 2018 [7–9].

Most of the around 4000 characterized nuclides are radioactive [10]. In many cases it is not possible to make radioactive nuclei targets and perform an experiment because of the short half-life of the nucleus of interest. To study these radioactive nuclei, RIBs are used on stable targets. One way of obtaining a RIB is to use the Isotope Separator On Line (ISOL) method. In the ISOL method, two accelerator systems are needed. The first accelerator is used to produce the radioactive atoms at rest, and the second accelerator is used to accelerate these atoms [11].

In RIB facilities the energy and intensity is generally lower compared to stable beam facilities. This makes it suitable for Coulomb excitation and particle transfer reactions. The beam is the isotope of interest and since it is traveling with a significant velocity (v/c values of a few percent), the emitted γ -rays from de-excitation may have large Doppler shifts. Since the detectors have a finite solid angle, it can lead to a sizable Doppler broadening. When the detection system has high granularity, the Doppler shifts and broadening can be corrected for. If the angle between the recoiling nucleus and the γ -ray can be determined accurately, Doppler correction can be applied [12].

3.1.1 Beam production

A continuous flow of accelerated proton beam bunches from the PSB comes into the ISOLDE facility and collide with a thick production target. The proton beam has an energy of 1.4 GeV and an intensity up to $2 \mu\text{A}$. Two proton beam bunches are separated by 1.2 s [14, 15]. ISOLDE typically takes 50% [12] of all proton bunches from the PSB, the rest goes to the Large Hadron Collider (LHC) and other experiments shown in [Figure 3.1](#). In the reaction between the proton beam and the production target, radioactive nuclides are produced in spallation, fission or fragmentation reactions (basically smashing the target into pieces) [8]. The production target is chosen from a stable region heavier than the nucleus of interest. In our experiment, a production target of tantalum (Ta) was used, producing the elements in the chart of nuclides up to Ta. A large amount of

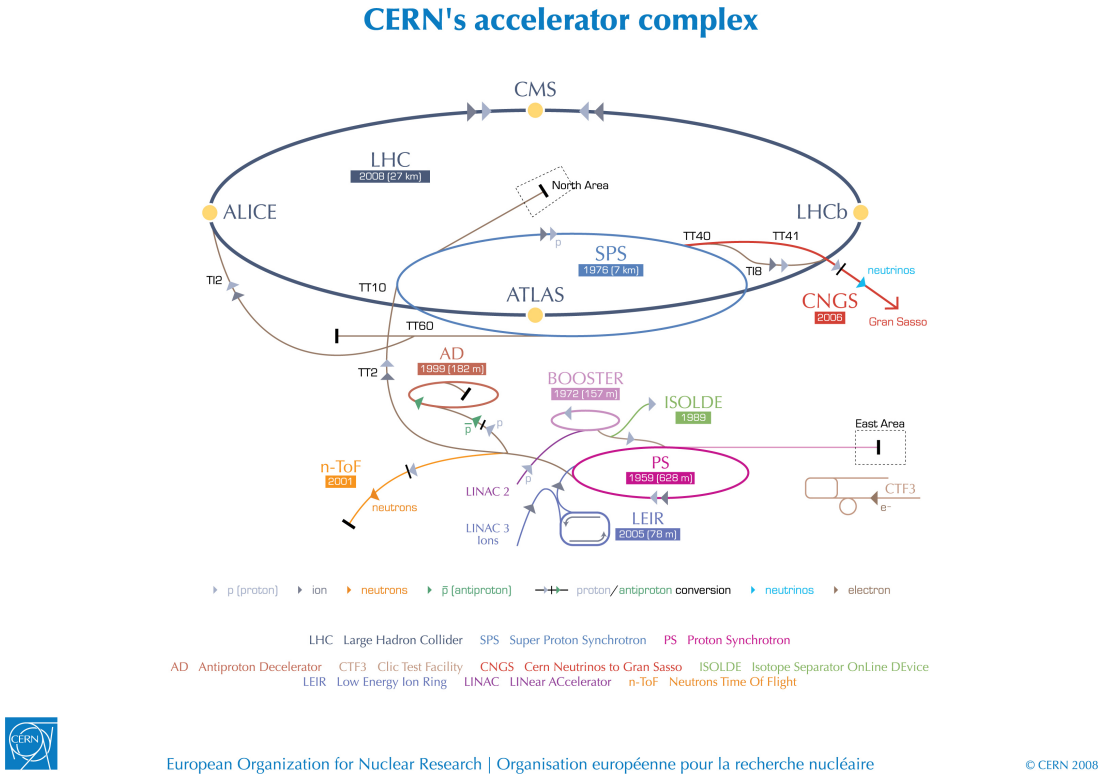


Figure 3.1: The CERN accelerator complex [13]. ISOLDE gets accelerated protons from LINAC 2 and the PS Booster.

different isotopes is produced in this way, and the challenge is to extract the nucleus of interest. To obtain the nucleus of interest, we first have to use a method of selecting the atom of interest, and then the nucleus of interest.

To get the atomic element of interest, one idea is to use a method of selective ionization and then a high voltage electrostatic field to extract the ions. Electronic transitions are characteristic for each chemical element. A laser with precisely tuned wavelength can obtain the photon energy that matches the electronic transition energies in the atom [16, 17]. Thus we can use one laser to excite an electron to a specific excited electron-state in the atom, a second laser to excite electrons further to another excited electron-state and a third laser to kick out the electron. In this way we only ionize the atomic element of interest. There could be contaminants from surface ionization (atoms that collide with the walls of the ion source), but this is detectable. Using periods of laser on and off, we can detect the resulting contaminants in the beam. The Resonance Ionization Laser Ion Source (RILIS) is based on the method of step-wise (2-3 step) excitation and ionization of the atom. It is an element-selective process which is used to produce ion beams of the correct element [18]. In this experiment RILIS was used to select samarium (Sm) with atomic number $Z = 62$.

At this point we have a continuous beam of Sm ions of 60 keV energy (the target is on a 60 kV high voltage platform) [8, 14]. The next step in the process is to have mass separation, and we need to give the continuous beam a fine structure, because the post-accelerator cannot accept a continuous beam coming in, it accelerates bunches. The beam can collide in one of two target stations, either the General Purpose Separator (GPS) or the High Resolution Separator (HRS). The GPS has one bending magnet and can deliver beams of different masses ($\pm 13\%$ of the central beam line mass) simultaneously into three beam lines, while the HRS has two bending magnets with high mass resolving power which delivers the beam into the main (central) beam line [14, 19]. In this experiment the GPS was used to select the isotope of Sm with mass number $A = 140$.

Now we have a continuous beam of ^{140}Sm . The mass separator also gets rid of contaminants that come out of RILIS but have different mass. There could still be isobaric contaminants from surface ionization but luckily there is very little surface ionization for the neighboring elements of Sm. In the Radioactive beam EXperiment TRAP (REXTRAP) we collect the ^{140}Sm ions, so that we can release them in bunches that are matched to the fine structure of the LINear ACcelerator (LINAC). REXTRAP is a penning trap which has the tasks of accumulation, bunching and cooling of the RIB [7, 20, 21]. The ions are released in bunches and transferred to the REX Electron Beam Ion Source (REXEBS).

REXEBS is a charge breeder where the RIB is bred to a high charge state [22], with a mass-to-charge (A/q) ratio typically between 2.5 and 4.5 [23]. REXEBS releases the beam with a certain energy through a mass separator and into the HIE-ISOLDE LINAC [7]. To accelerate the charged ions (the beam) to high energy, we need highly charged ions. The EBIS blasts off more electrons from Sm, which leaves the nucleus in a high charge state, going from $^{140}\text{Sm}^{+1}$ to $^{140}\text{Sm}^{+34}$ ($A/q \approx 4.1$). The longer the ions stay in REXEBS, the higher the charge state becomes. We get a distribution of charge states, and we loose those that have the wrong charge state because the LINAC can only accept one charge state [24–27].

The HIE-ISOLDE LINAC accelerates the beam of ^{140}Sm to 4.65 MeV/u through the beam line, and magnets bend the beam into the Miniball spectrometer, where the particles and γ -rays are detected. This experiment was one of the first Miniball experiments with the new upgraded superconducting accelerator.

To have a successful experiment, the purity of the beam is of great importance. Contaminants in the beam can come from different sources [12]. From the primary target we can have:

- isobaric contaminants which are inseparable by the mass separator because of the same mass number
- isotopes with an integer multiple of both mass and charge

and from stable isotopes the contaminants can come from:

- buffer gas in REXTRAP (e.g. Ne, Ar)
- residual gas in REXEBIS (e.g. C, O)
- components of REXEBIS (e.g. La from the cathode)

3.1.2 Target

As a target, ^{208}Pb with a thickness of 1.4 mg/cm^2 was chosen. The reason for the choice is that it is very hard to excite ^{208}Pb since it's doubly magic. We wanted the highest possible Z ($= 82$) of a stable isotope to get maximum excitation probability.

Since we don't need normalization (because we have the $B(E2, 0_1^+ \rightarrow 2_1^+)$ from the previous experiment [4] and from lifetime measurement [28]), we have chosen a target that is very hard to excite, so transitions from the target will not complicate the spectrum.

^{208}Pb has no quadrupole deformation, the first excited state ($2615 \text{ keV}, T_{1/2} = 16.7 \text{ ps}$) is of octupole vibration ($J^\pi = 3^-$). If we are **lucky/unlucky?** we might see a little bit of this first excited state in the spectrum. This happens if the "collision" is almost head on, and the target hits one of the inner rings.

Unfortunately there was a finger print on the target, so even before beginning the experiment, we have some contamination (probably carbon). The target wheel is shown in [Figure 3.2](#).

3.2 Miniball spectrometer

3.2.1 Target chamber

In Coulomb excitation experiments the target chamber is surrounded by the γ detectors as shown in [Figure 3.4](#). The chamber is a hollow sphere made out of a machined out, single piece of AlMg_3 , with a thin wall and an inner radius of approximately 80 mm. Inside the chamber we find a target wheel and a particle detector. The target wheel can hold up to six different targets as shown in [Figure 3.2](#). The particle detector can be positioned 25 - 31 mm from the target wheel, limited by the space inside the chamber. Outside of the target chamber the average distance from each γ -detector cluster to the center of the target chamber is approximately 10 cm. The forward detectors and the backward detectors has an angular position θ of approximately 45° and 135° respectively, compared to the beam line. In the vertical plane ϕ , perpendicular to the beam line, the four γ -detectors in forward and backward position are placed roughly on a circle with a separation of 90° [12].

3.2.2 Particle detector, DSSSD (CD)

To detect the scattered beam and target nuclei, a segmented double sided silicon strip detector (DSSSD) composed of four quadrants was used. The DSSSD looks very like an audio compact disc (CD), and hence it is called the CD. In the front of the CD, one quadrant consists of 16 annular strips (rings) with a pitch of 2 mm, while the back consists of 24 sector (radial) strips with a pitch of 3.5°. The innermost strip has an inner radius of the active area of 9 mm, while the outermost strip has an outer radius of the active area of 40.9 mm. There are in total 160 discrete detector elements for all four quadrants (64 in front, 96 in back). Each quadrant is connected to its own analog to digital converter (ADC). Because of lack of available channels in the ADC, the sector strips in the back are paired up, so that it is effectively 12 sector strips in the back side. The CD detector has a total area of 5000 mm², where the active area is approximately 93%. The silicon wafer thickness is between 50 μm and 1000 μm with a dead layer of 0.3 to 0.8 μm aluminum (Al) equivalent ([what does this mean?](#)). For simplicity the dead layer thickness is usually assumed to be 0.7 μm silicon (Si) equivalent ([what does this mean?](#)) [12, 29]. [Table 3.1](#) shows some of the specifications of the CD and [Figure 3.5](#) shows a sketch of the front and back side. The distance from the target to the CD is 26.98 mm (± 1 mm). In the laboratory (LAB) reference frame the CD has a angular coverage between 18.4° and 56.6°. [Table 3.2](#) shows the mid strip CD angles in the laboratory frame for the front of the CD. An extensive description of the CD can be found in [30].

Table 3.1: CD specifications.

Ring number	Annular strips (CD Front)	Sector strips (CD Back)
Number of strips	16	24
Inner radius of active area	9.000 mm	-
Outer radius of active area	40.900 mm	-
Strip pitch	2.000 mm	3.5°
Strip width	1.900 mm	3.4°
Strip length	-	31.900 mm
Active angle coverage	81.6°	-
Inner strip distance	-	0.100 mm

3.2.3 γ detectors, high-purity germanium (HPGe)

The γ -ray spectrometer consists of a total of 24 six-fold segmented high-purity germanium (HPGe) crystals, which are divided into 8 clusters of 3 crystals each. Each crystal encapsulated and segmented into 6 parts, making a total of 144 segments. For maximum efficiency, the detectors are placed in a compact geometry

Table 3.2: Mid ring CD angles in laboratory frame with distance from target to CD of 26.98 mm. The centroid energy is from simulation with kinsim3. E_t is the energy of the target particle and E_b is the energy of the beam particle.

Ring number	Mid ring distance [mm]	Angle [°]	E_t [MeV]	E_b [MeV]
0	40	56.0	139.62	273.80
1	38	54.6	151.51	286.78
2	36	53.1	164.55	299.11
3	34	51.6	182.41	312.31
4	32	49.9	198.95	326.87
5	30	48.0	219.53	342.40
6	28	46.1	240.36	358.75
7	26	43.9	262.77	376.35
8	24	41.7	287.31	395.31
9	22	39.2	313.65	414.84
10	20	36.5	340.64	435.42
11	18	33.7	369.54	456.71
12	16	30.7	398.95	478.33
13	14	27.4	428.87	499.72
14	12	24.0	457.53	520.55
15	10	20.3	484.86	539.89

around the target chamber [12, 31]. The detector-array can cover a solid angle of about 60% of 4π , when the optimum distance between the target chamber and the HPGe-clusters is achieved. The average energy resolution at $E_\gamma = 1.3$ MeV is 2.3 keV [32]. From each detector we get seven signals in total for each event, one from the core and six from each segment. **This requires 168 channels for data aquisition.** The shapes of these signals is analyzed to get information of the position. Because of the segmentation of the detector, a better Doppler correction can be performed compared to using the whole crystal. During operation the HPGe-clusters needs to be cooled by liquid nitrogen and there is an automated filling system in place for this [31].

3.3 Experimental setup

^{140}Sm Coulomb excitation experiment.

From operators logbook: 140Sm34+ at 4.65 MeV/u experiment. A/q = 4.0.

For Miniball geometry (angles) [33].

Experiment code: IS558

Ta: tantalum ($Z = 73$)

Sm: samarium ($Z = 62$)

Table 3.3: Geometry to the center of the Miniball HPGe clusters (red dot in Figure 3.7) for the Doppler correction.

Cluster	θ_i [°]	ϕ_i [°]	α_i [°]	R_i [mm]
0	311.16	126.67	129.79	107.08
1	51.08	62.74	51.83	100.59
2	309.02	126.87	51.23	105.76
3	251.90	57.44	130.31	105.40
4	296.93	235.53	128.74	106.48
5	233.45	239.09	46.67	105.18
6	59.42	308.67	131.04	127.04
7	130.56	309.09	46.46	110.18

Pb: lead ($Z = 82$)

Beam: ^{140}Sm ($T_{1/2} = 14.82$ min, 4.65 MeV/u, total 651 MeV), excellent purity

Target: ^{208}Pb (Thickness: 1.4 mg/cm²)

Small angle: Forward scattering: Larger distance, weaker EM-field, less excitation probability.

Large angle: Backward scattering: Closer distance, stronger EM-field, higher excitation probability.

Expect to measure transition probabilities $B(E2)$ and quadrupole moment (nuclear deformation).

3.4 Data acquisition system

Signals from the CD and the HPGe clusters are read out by the ADC and DGF modules and sent to a personal computer (PC) in the data acquisition (DAQ) room at ISOLDE where the data is then stored. The collection of data is done by the MAR_aBQU [34] DAQ system [12]. It is split in two parts as shown in Figure 3.9, one front-end part based on the multi branch system (MBS) [35] and one back-end part based on the ROOT framework [36]. The front-end takes care of data readout, event building and data transportation, while the back-end takes care of the setup, run control, histogramming, data analysis and data storage [12].

Other info sources:

- MAR_aBQU web page: <https://www-old.mll-muenchen.de/marabou/html/doc/>
- MAR_aBQU file formatting: <https://www-old.mll-muenchen.de/marabou/html/doc/marabou/IOSpec.html>

Table 3.4: LAB vs CM. Based on LAB input angles from θ_b and θ_t . From LISE++ kinematics calculator (reaction from the middle of the target).

(a) $\theta_b \in [22.0^\circ, 56.7^\circ]$.			(b) $\theta_t \in [22.0^\circ, 56.7^\circ]$.		
LAB	CM		LAB	CM	
θ_b [°]	θ_t [°]	θ'_b [°]	θ_b [°]	θ_t [°]	θ'_b [°]
22.0	71.7	36.6	40.6	56.7	66.6
26.0	68.4	43.2	42.3	55.3	69.4
29.1	65.9	48.2	44.2	53.9	72.2
32.2	63.4	53.3	46.1	52.4	75.2
35.2	60.9	58.1	48.3	50.7	78.6
37.9	58.8	62.4	50.6	49.0	82.0
40.4	56.8	66.3	53.1	47.1	85.8
42.8	54.9	70.1	56.0	45.0	90.0
45.0	53.2	73.5	59.1	42.8	94.4
47.1	51.6	76.7	62.5	40.4	99.2
49.0	50.2	79.6	66.1	37.9	104.2
50.7	48.9	82.1	70.2	35.2	109.6
52.4	47.6	84.7	75.0	32.2	115.6
53.9	46.5	86.9	80.2	29.1	121.8
55.3	45.5	88.9	85.8	26.0	128.0
56.7	44.5	91.0	93.8	22.0	136.0

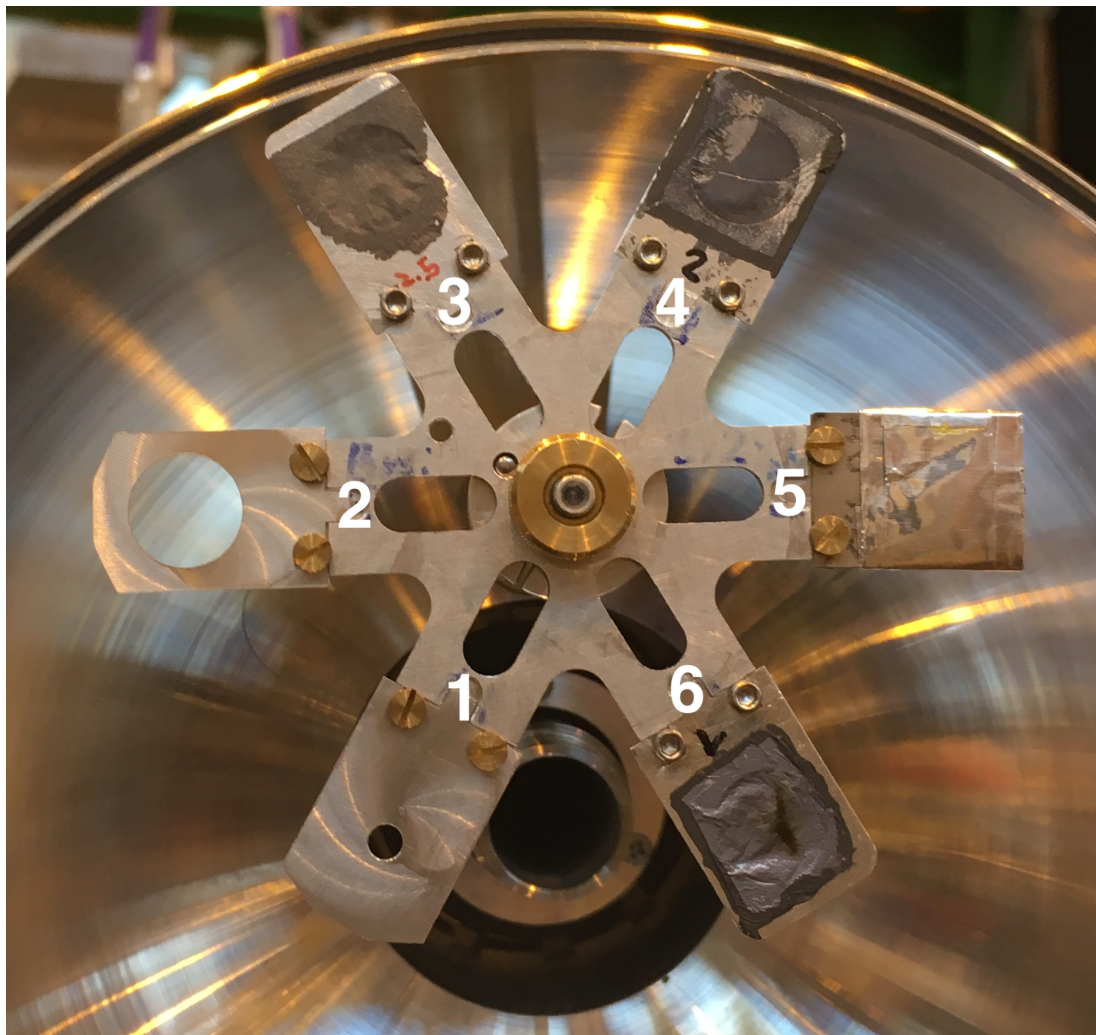


Figure 3.2: The target wheel can hold up to six different targets. Position 6 has the target ^{208}Pb with thickness 1.4 mg/cm^2 . Photo by: Liam Gaffney, date: 07.08.2017.

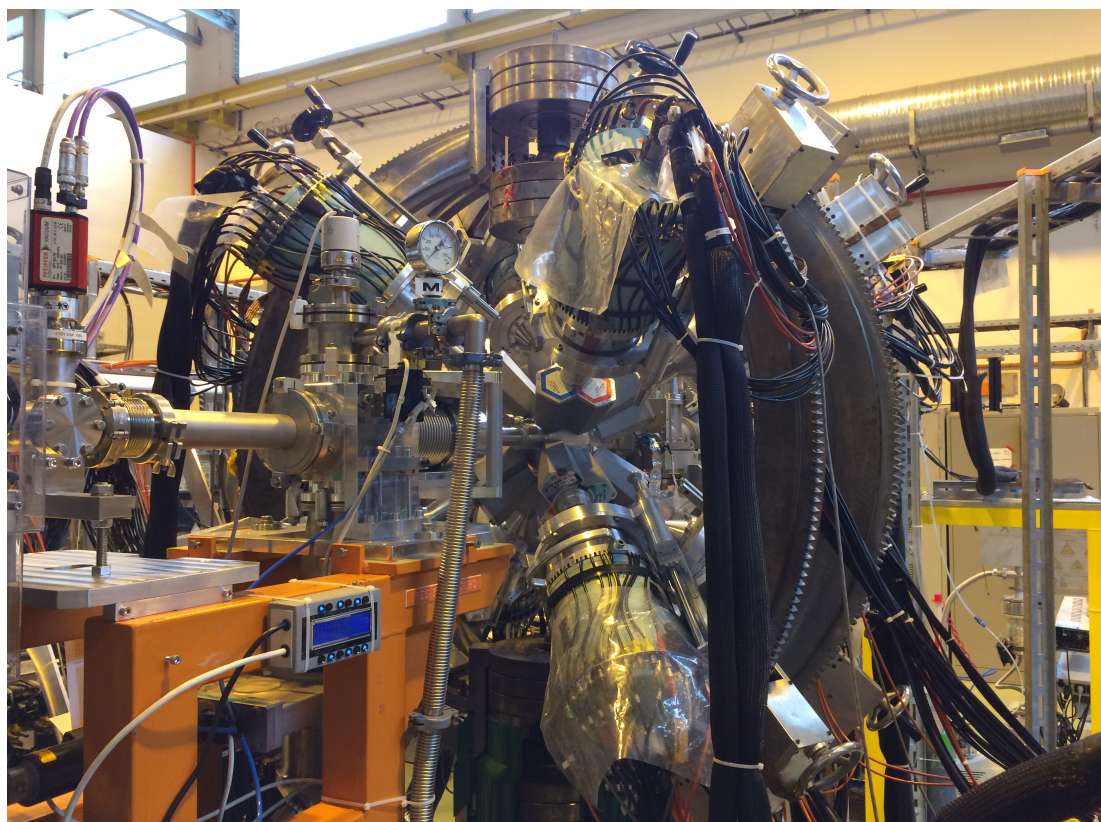


Figure 3.3: Overview picture of the Miniball spectrometer. Photo by: Trond Wiggo Johansen.

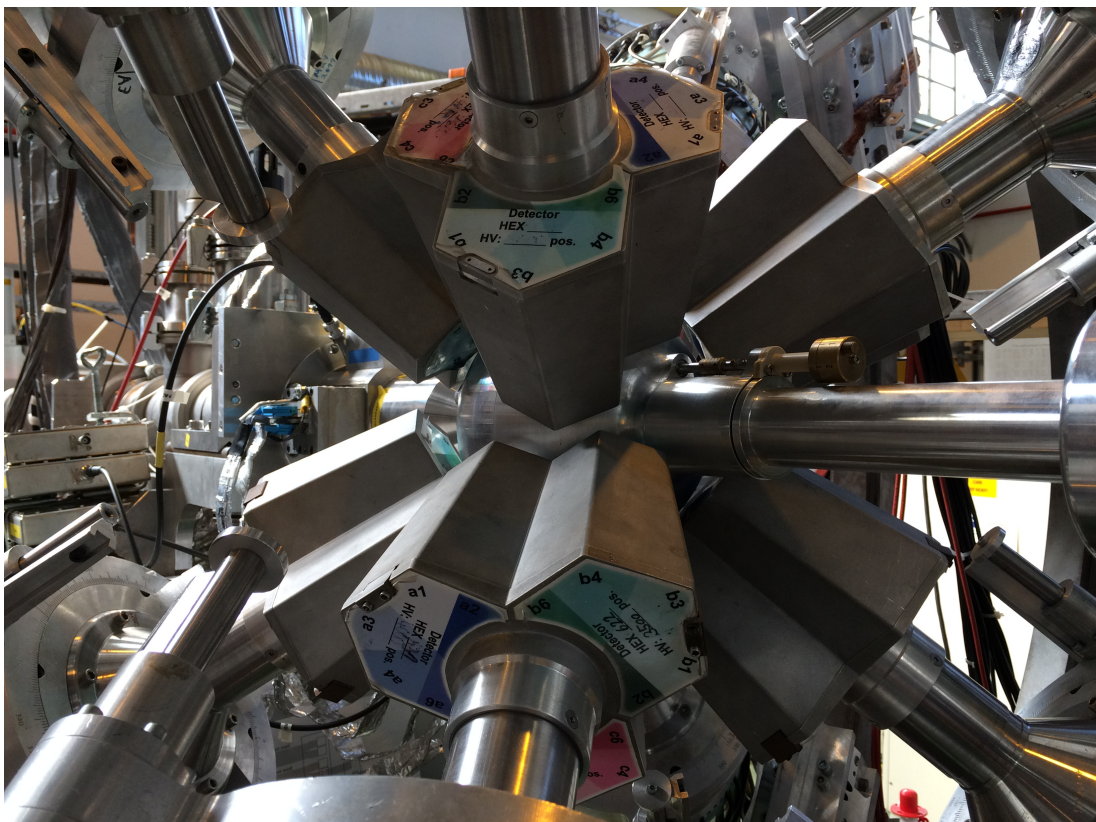
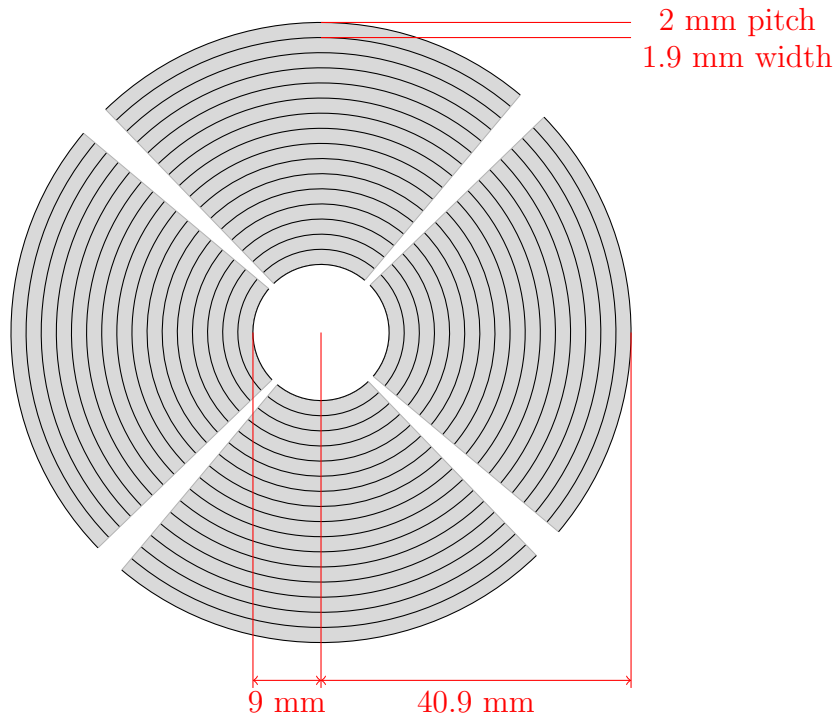
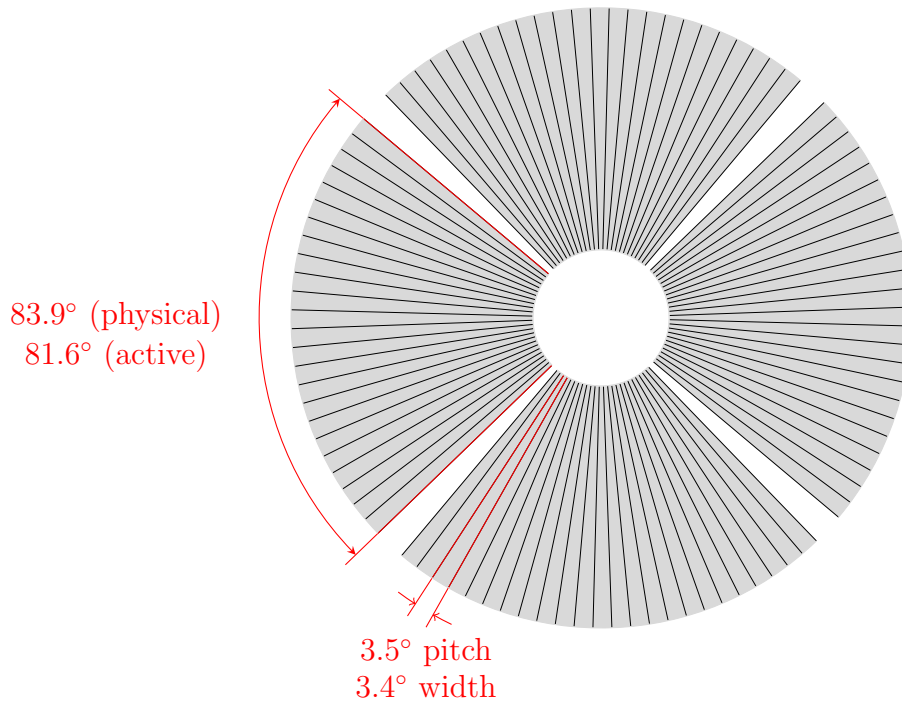


Figure 3.4: Close up picture of the Miniball spectrometer. The Miniball target chamber is in the middle, surrounded by the triple-cluster encapsulated γ crystals. The beam line goes through the target chamber. Photo by: Trond Wiggo Johansen.



(a) CD front: The numbering of the strips goes from strip 0 (outermost) to strip 15 (innermost). Quadrants are numbered in clockwise direction with respect to the beam direction, so that left is 1, up is 2, right is 3 and down is 4.



(b) CD back: The numbering of the strips goes from strip 0 to strip 23 in counter-clockwise direction viewed from this side. Quadrants are numbered in clockwise direction with respect to the beam direction. From this perspective right is 1, up is 2, left is 3 and down is 4.

Figure 3.5: CD sketch, adapted from [29].

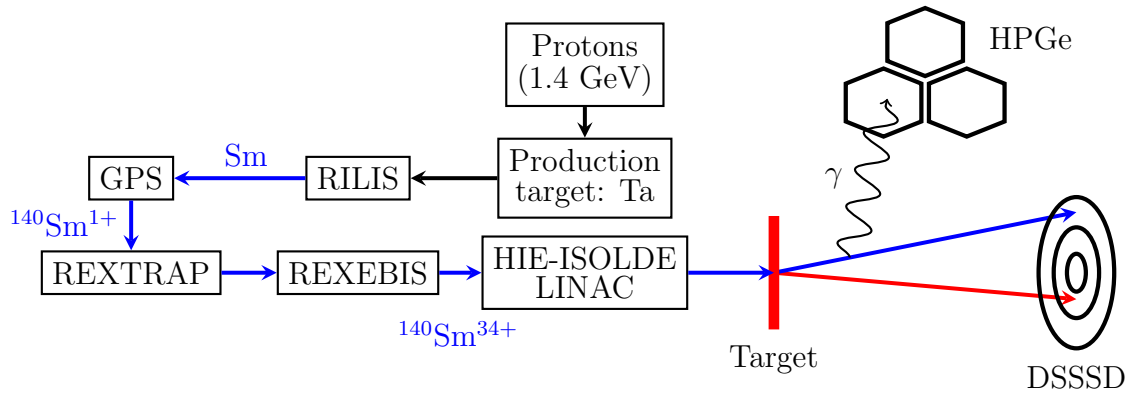


Figure 3.6: The Coulomb excitation setup at ISOLDE. Adapted from Malin Klintefjord's PhD thesis [1].

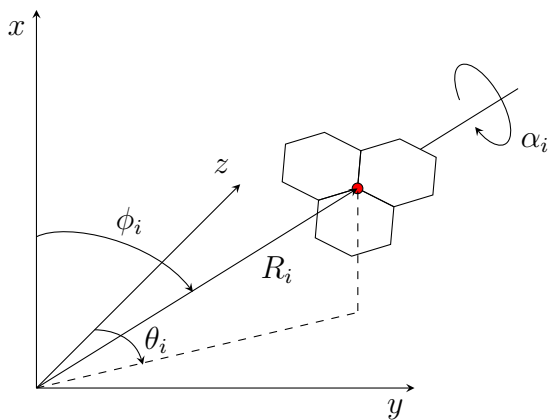
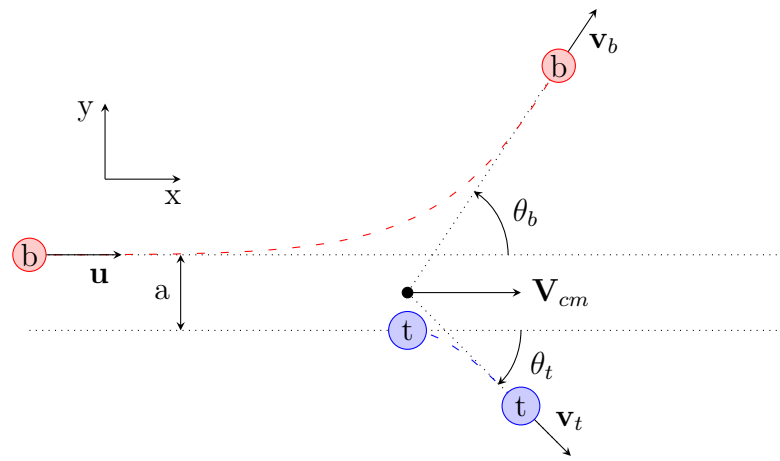
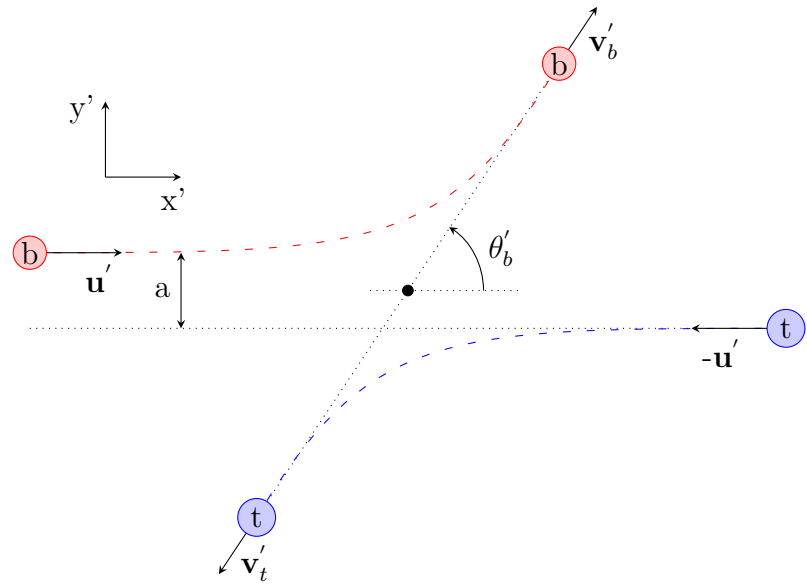


Figure 3.7: Miniball angles, where i denotes cluster number from Table 3.3.



(a) Laboratory (LAB) frame



(b) Center of mass (CM) frame.

Figure 3.8: LAB vs CM frame.

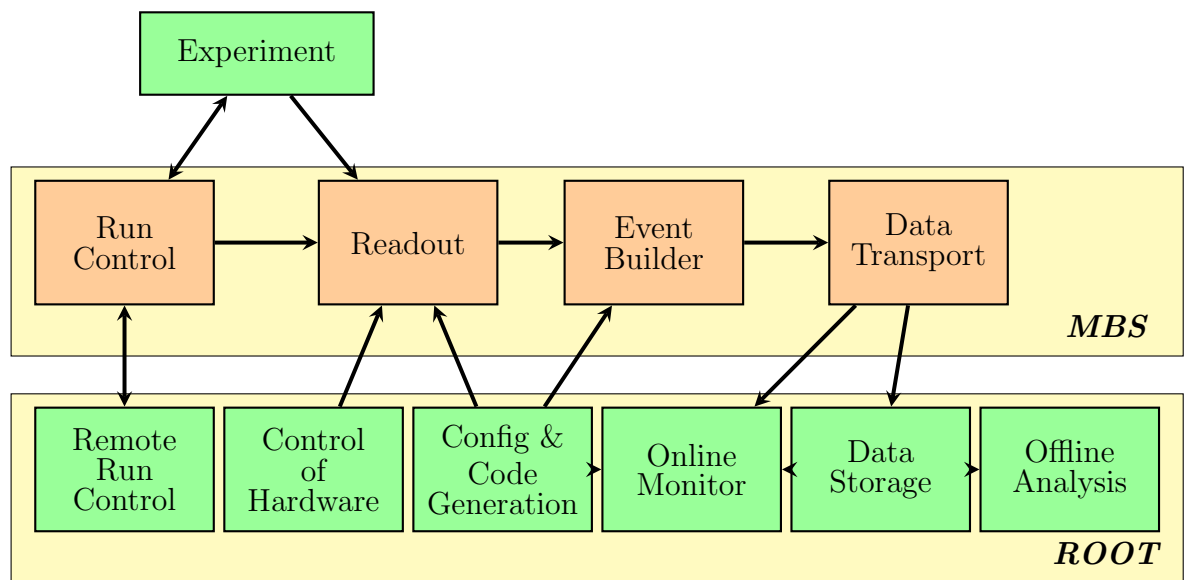


Figure 3.9: MAR_aBQU tasks, adapted from [34].

Chapter 4

Data analysis

Tilbakemelding:

First: explain the tasks and give the bigger picture of what needs to be done:
starting point: Raw data in list mode: ID, E, T, ID, E, T, ... (basically)
what you want: Doppler-corrected γ -spectra with various conditions on particles,
angles, etc.

procedure: 3 steps:

1. convert raw data to ROOT format
 2. event-building:
 - calibrate detectors, apply thresholds, etc.
 - use correlations to build events: particle- γ coincidences
 - store everything in a tree structure for easy access
 3. apply gates on particles and perform Doppler correction
-

Could be nice to have a "cook book", i.e. step-by-step explanation of this procedure.

ROOT: analysere data [36]

kinsim3 [37] + SRIM [38]

MiniballCoulexSort [39]

Table 4.1: Computer used for data analysis

Model	MacBook Air (13-inch, 2017)
Processor	1.8 GHz (Intel Core i5)
Memory	8 GB (1600 MHz DDR3)

Run time for sorting data:

TreeBuilder (online calibration): \sim 40-45 min

AQ4Sort (online calibration): \sim 120 min

Table 4.2: Run time for sorting data.

Executable	Run time [min]
TreeBuilder	~ 45
AQ4Sort	~ 120

The run time of the bash script was done with the built in script time

```
$ time ./AQ4S.sh Sm online TB
...
real 45m19.265s
user 42m49.653s
sys 0m39.665s
```

```
$ time ./AQ4S.sh Sm online Q4
...
real 121m40.830s
user 116m18.361s
sys 1m17.809s
```

```
$ time ./AQ4S.sh Sm user TB
...
real 41m11.282s
user 39m45.592s
sys 0m27.777s
```

```
$ time ./AQ4S.sh Sm user Q4
...
real 143m47.600s
user 128m6.174s
sys 1m50.921s
```

MedToRoot: file 9

```
$ ./M2R.sh Sm
opening file ../../Raw_data/Sm/140Sm_208Pb_pos6_009.med ...
EventBuffer::EventBuffer(GlobalSettings *)
Processing event number      0
Start trigger #14

Processing event number    40000
Stop trigger #15
```

```

Unpacked 47268 events:
wrong dgf hit pattern:          0 ( 0.0 %)
wrong adc headers:             0 ( 0.0 %)
# of overflows in adc channels: 147009 (311.0 %)
# of underflows in adc channels: 0 ( 0.0 %)
pattern unit mismatches:       0 ( 0.0 %)

Number of ebis pulses:           23584
Number of t1 pulses:              717
Number of supercycle pulses:      153
committed           351 320 654 bytes to tree tr, 'Tree for on
beam data of Coulex setup@Miniball'
and                 4 889 999 bytes to tree bg, 'Tree for on
beam background data of Coulex setup@Miniball'
and                 68 650 177 bytes to tree tr, 'Tree for off
beam data of Coulex setup@Miniball'
wrote                63 916 bytes to file ../../Raw_data/Sm
/140Sm_208Pb_pos6_009_OnBeam.root => compressed by a
factor of 5496.6
,                  9 451 bytes to file ../../Raw_data/Sm
/140Sm_208Pb_pos6_009_OnBeamBackground.root => compressed
by a factor of 517.4
,                  44 809 bytes to file ../../Raw_data/Sm
/140Sm_208Pb_pos6_009_OffBeam.root => compressed by a
factor of 1532.1
and                12 904 bytes to file ../../Raw_data/Sm
/140Sm_208Pb_pos6_009_Scaler.root => compressed by a
factor of 1690.2

```

MedToRoot: file 25

```

$ ./M2R.sh Sm
opening file ../../Raw_data/Sm/140Sm_208Pb_pos6_025.med ...
EventBuffer::EventBuffer(GlobalSettings *)
Processing event number      0
Start trigger #14

```

```

Processing event number 100000
Stop trigger #15

```

```

Unpacked 105352 events:
wrong dgf hit pattern:          0 ( 0.0 %)
wrong adc headers:             0 ( 0.0 %)
# of overflows in adc channels: 535143 (508.0 %)
# of underflows in adc channels: 0 ( 0.0 %)
pattern unit mismatches:       0 ( 0.0 %)

Number of ebis pulses:           52626
Number of t1 pulses:              1904
Number of supercycle pulses:      150

```

```

committed      1 68 292 586 bytes to tree tr, 'Tree for on
beam data of Coulex setup@Miniball'
and           12 475 16 bytes to tree bg, 'Tree for on
beam background data of Coulex setup@Miniball'
and           213 620 380 bytes to tree tr, 'Tree for off
beam data of Coulex setup@Miniball'
wrote         95 604 bytes to file ../../Raw_data/Sm
/140Sm_208Pb_pos6_025_OnBeam.root => compressed by a
factor of 11174.1
,           16 636 bytes to file ../../Raw_data/Sm
/140Sm_208Pb_pos6_025_OnBeamBackground.root => compressed
by a factor of 749.9
,           64 319 bytes to file ../../Raw_data/Sm
/140Sm_208Pb_pos6_025_OffBeam.root => compressed by a
factor of 3321.3
and           20 646 bytes to file ../../Raw_data/Sm
/140Sm_208Pb_pos6_025_Scaler.root => compressed by a
factor of 2080.6

```

TreeBuilder

```

$ ./Q4S.sh Sm user TB
—— TreeBuilder ——
input file(s):
... <shows a list of all input files>
output file: Sm_user-TreeBuilder-2019-06-20.root
calibration file: ../../Miniball-config/IS558-user.cal
WeightPR: 0.75
Particle distribution:
Q0 fired: 12243817
Q1 fired: 12277727
Q2 fired: 11479362
Q3 fired: 10936096
Finished.

```

AQ4Sort

```

$ ./Q4S.sh Sm user Q4
Info: No flag option for 'AQ4Sort'. Ignoring optional flag.
—— AQ4Sort ——
calibration file: ../../Miniball-config/IS558-user.cal
input file(s):
... <shows a list of all input files>
output file: Sm_user-AQ4Sort-2019-06-24.root

```

CLXAna

```
$ ./Coulx.sh -n
--- Coulx: normal ---
Input parameters:
Zb = 62
Ab = 140
Zt = 82
At = 208
Eb = 4650 keV/u
Ex = 531 keV
thick = 1.4 mg/cm2
depth = 0.7 mg/cm2
cddist = 26.98 mm
cdoffset = 242.6 degrees
deadlayer = 0.0007 mm
contaminant = -1 mg/cm2
spededist = 23.6 mm
bg_frac = -0.75
srim = /Users/trondwj/GitHub/MasterThesis/SRIM
cutfile = ../../Sorted_data/outputfile.root:Bcut:Tcut
Begin g_clx loop.
Info in <TCanvas::Print>: pdf file /Users/trondwj/GitHub/
    MasterThesis/SRIM/140Sm_208Pb.pdf has been created
Info in <TCanvas::Print>: pdf file /Users/trondwj/GitHub/
    MasterThesis/SRIM/208Pb_208Pb.pdf has been created
Info in <TCanvas::Print>: pdf file /Users/trondwj/GitHub/
    MasterThesis/SRIM/140Sm_Si.pdf has been created
Info in <TCanvas::Print>: pdf file /Users/trondwj/GitHub/
    MasterThesis/SRIM/208Pb_Si.pdf has been created
Initialising histograms...
Looping over events...
Warning in <TClass::Init>: no dictionary for class trevts is
    available
1-particle events = 89020258%
Finished.
```

hadd

After saving "part" from CLXAna-file:

```
$ cd GitHub(ROOT-framework/build/bin
$ hadd /Users/trondwj/GitHub/MasterThesis/Sorted_data/
    outputfile.root /Users/trondwj/GitHub/MasterThesis/
    Sorted_data/part.root /Users/trondwj/GitHub/MasterThesis/
    Sorted_data/Bcut.root /Users/trondwj/GitHub/MasterThesis/
    Sorted_data/Tcut.root
```

•

particle-gamma and particle-gamma-gamma coincidence
 sjekk opp om energi fra online kalibrering passer med simuleringen.

4.1 Data and sorting

4.1.1 Digital electronics - unnecessary?

The Miniball spectrometer [12]

p. 7:

Digital electronics:

left top:

This means that the FPGA (field programmable gate arrays) can cope with high counting rates with no dead time and is essentially limited only by pile-up.

left bottom:

These buffers contain the energies of the γ -rays, 48 bit time stamps with 25 ns resolution and either the time to steepest slope or the mirror charge, for each of the 168 channels. This buffer size is large enough that the DGF-4Cs only need to be read out between beam bursts, so the readout does not produce additional dead time.

right top:

ADCs and TDCs are capable of buffering up to 32 events.

Gamma:

core ID from 0 to 23

segment ID from 0 to 6 (zero is the core)

cluster ID from 0 to 7

ADC:

annular (front) strip ID of particle (0 = outer; 15 inner)

secular (back) strip ID of particle (0 to 12; clockwise wrt beam)

[From offl_root_med.pdf](#)

”Direction of the central axis of the detector (r, θ, ϕ) and the notation about the axis of the cluster (α), [is this correct??](#). Needed to calculate the positions of the segments or the position of a point determined by the pulse-shape analysis.

In order to perform the Doppler shift, we need to know the angle in the Miniball frame of reference of the interaction point. We determine the interaction point either from the segment with the largest energy or using pulse-shape

analysis. In the former case, we need to know the position of the centre of each segment. In the latter, we need geometrical information to relate the time-to-steepest slope and ratio of the mirror charge amplitudes to the angle between the interaction point, the target and the emitted particle.”

The analysis code for Miniball data is named MiniballCoulexSort and is available on GitHub at <https://github.com/Miniball/MiniballCoulexSort>. The main steps of how to download, install and use it is outlined in the README.md file in the GitHub repository.

Data from Miniball comes in the form of .med-files (Miniball Event Data). In order to analyze this data in ROOT¹ the first part of the sorting is just to convert the .med-files into .root-files with the script MedToRoot.

To get useful information out of the converted .root-files, the Treebuilder script is used. The .root-file(s) and a calibration file is given to the Treebuilder so it can make event trees that can be used for analyzing the Coulomb excitation events.

One script that is mentioned in the Miniball GitHub repository, but not showed how to use, is the AQ4Sort. It is used in the same way as the TreeBuilder script, but it sorts the histograms in another way. This script is used before and during the calibration of the detectors, because it gives information about every single ring and every single back strip. The one thing to note here, is that the numbering of the detector rings and strips are different from the ones used in Treebuilder.

The histograms sorted by Treebuilder starts counting from 0 and the AQ4Sort starts counting from 1.

The ADC spectras from the file sorted by Treebuilder have a naming convention of adc_q_s, where q corresponds to the quadrant and s corresponds to the channel. The front energy is saved in adc_[0-3]_[0-15] and the back energy from strips 1-12 from all 16 rings (the whole quadrant) is saved in adc_[0-3]_[16-27].

Tilbakemelding:

useful with a table that explains all the different channels and assigns the various detector segments/rings? (naming conventions) (appendix?)

adc_0_0 in the file sorted by Treebuilder is the same as fE_Q1_f1 sorted by AQ4Sort. All the front detectors can be found in the Treebuilder-sorted file, but when it comes to the back detector, the single pixels from the strips are not shown. These are available through the AQ4Sort sorted file. For the front detectors the histograms adc_[0-3]_[0-15] and fE_Q[1-4]_f[1-16] are the same. For the back detectors, we have that adc_[0-3]_[16-27] and bE_Q[1-4]_b[1-12] are the same. In addition in AQ4Sort we can see the different pixels. The histograms fE_Q[1-4]_f[1-16]_b[1-12] shows the front energy of quadrant 1-4 gated on ring 1-16 and back strip 1-12, while the bE_Q[1-4]_f[1-16]_b[1-12] shows the same, only for the back energy.

¹ROOT is a data analysis framework made at CERN.

Tilbakemelding:

a little confusing: is it correct that the treebuilder sort individual spectra for the front and back strips, but if you want coincidences between front and back (\rightarrow pixels) you use AQ4Sort?

In the naming convention of `adc_q_s` or `fE_Qu_fv`, where $q \in [0, 1, 2, 3]$, $s \in [0, 1, \dots, 27]$ and $u \in [1, 2, 3, 4]$, $v \in [1, 2, \dots, 16]$, the $s = 0$ and $v = 1$ is the outermost ring, while $s = 15$ and $v = 16$ is the innermost ring. In our case, the innermost ring was so destroyed that we have to remove it from the data analysis.

`adc_q_s`, where $q \in [0, 1, 2, 3]$, $s \in [0, 1, \dots, 27]$.

`pE_Qq_fr_bs`, where $\in [b, f]$, $q \in [1, 2, 3, 4]$, $r \in [1, 2, \dots, 16]$ and $s \in [1, 2, \dots, 12]$.

The `adc[0-3][16-27]` or `bE_Q[1-4].b[1-12]` are a combination of all the 16 rings of `bE_Q[1-4].f[1, 2, \dots, 16].b[1-12]`.

Don't blame me for the naming convention, I did not write the code. I just tried to make sense of it.

4.1.2 ???

The Miniball spectrometer [12]

p. 8:

Efficiency and resolution: left bottom:

The application of an add-back (AB) routine involves the summing of the energies of two coincident gamma rays within 100 ns in neighboring cores on the same cluster detector. This situation corresponds to a Compton-scattered γ -ray event where the energy of the γ -ray is shared between two or more crystals in the same triple cluster detector. For higher-energy γ -rays, where scattering from one crystal into its neighbor is quite likely, this improves the efficiency, but for low-energy γ -rays, where scattering is less likely, summing effects actually reduce the efficiency. For this reason a cut-off is normally applied and AB is only performed for energies above this threshold.

4.2 Helping scripts

All of my scripts are available in the GitHub repository <https://github.com/wiggoen/MasterThesis>.

In order to not copy and paste the sorting command in the terminal for every data file, I made two bash scripts to do this. The script **M2R.sh** is using MedToRoot to take in as many files as you want, and sort it in one go. The other script is **AQ4S.sh**, which is using either AQ4Sort or Treebuilder to sort a lot of files in one go.

Tilbakemelding:

you should have a list of all the files with comments: in-beam data, calibration,

laser on-off, problems, which ones can be used and which can not.

I also made other helping scripts to get histograms, do fitting, comparison and calibration.

My scripts: MultiFit.cpp, MultiPlot.cpp, ++ (python, bash,..)

Tilbakemelding:

if you try to write this step-by-step cook book, you could introduce your scripts wherever is the right place to use them.

4.3 Simulation

To calibrate the data, we need to know the expected energy of the centroids of the peaks. This was done by simulating the experiment in a program called kinsim3. The program is written by Liam Gaffney² and the purpose of the program is to simulate the kinematics of the experiment. It takes into account the Silicon dead layer.

kinsim3 generates pdf-files of the stopping powers automatically. The rest of the plots are available inside the root-file. To get the energy simulation for each ring, the function `cd_sim_plots()` from the script **MultiPlot.cpp** was used.

Tilbakemelding:

what are the ingredients for this simulation?

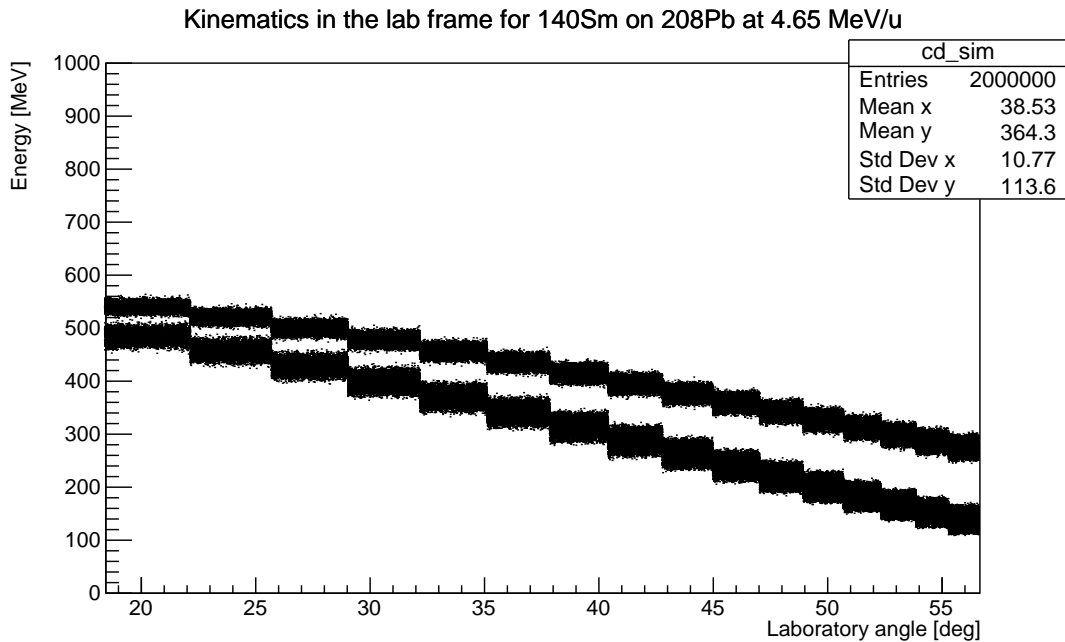
simple 2-body kinematics: energy of projectile, scattering angle of projectile \Rightarrow energy of scattered projectile, {angle, energy} of binary partner (target recoil)
Stopping powers (which models?) \rightarrow SRIM

Slowing of the particles in the target and in the dead layer of Si

CD to target distance: 26.98 mm.

Simulation done by kinsim3

²Liam Gaffney is a fellow at ISOLDE, affiliated with MINIBALL.



Tilbakemelding:

explain figure: Sm/Pb inner ring, Sm/Pb outer ring
 simulation does not consider cross sections: in simulation all angles are equally probable. The corresponding figure from your data looks therefore quite different.

— Mail from Liam started —

”the source has a thickness of 1.23 mm, which needs to be factored in so that the CD to target distance is the CD to source distance PLUS the source thickness, i.e. $25.78 \text{ mm} + 1.23 \text{ mm} = 27.01 \text{ mm}$. This is very close to the 26.98 mm you got from us in August. I think that the source data was reanalysed since the original blog entry, giving the 0.03 mm difference!”

— Mail from Liam ended —

Terminal: Simulation: ^{140}Sm on ^{208}Pb :

```
$ cd GitHub/Miniball/kinsim
$ root
root [0] .L kinsim3.cc+
root [1] kinsim3(62, 82, 140, 208, 1.4, 4.65, 0.02, 1.0, 0.6,
  26.98, false, 1e6, "../SRIM")
```

kinsim3 function:

```
void kinsim3( int Zb, int Zt, double Ab, double At, double
  thick /* mg/cm^2 */, double Eb /* MeV/u */ ,
```

```

    double dEb = 0.1 /* MeV/u */ , double Ex = 1.0 /* MeV */ ,
    double res = 0.6 /* % */ ,
    double cd_dist = 28.0 /* mm */ , bool flat = false /* angular
        distribution? */ ,
    long Nevts = 1E6, string srim_dir = "./srim" )

```

Say something about SRIM files.

4.4 Calibration

Tilbakemelding:

start with explaining the general idea for the calibration:

determine centroids of peaks in spectra, compare with simulations (kinematics, energy loss) to get linear coefficients (gain + offset). You could show spectra for 2 rings: one where it is ok to get the 2 centroids for Sm and Pb, and one where it is difficult → use additional data (Ni?)

Sectors: cover wide angular range → no sharp peaks

Solution: gate on rings to see peaks in sectors and calibrate.

Idea:

1. produce spectra
2. set thresholds: example, explain criteria
3. find calibration coefficients → see above
explain strategy, show examples...
4. time calibration

My goal of the calibration was to make a program that could automatically fit the plots i needed, but it became more and more manual labor. Because of the shape of the data peaks, it demands very much individual care. This I could not do with a automatic program. The downfall of the automatic centroid collector came when trying it on the back detectors.

The total amount particle front detectors to calibrate is 4 quadrants * 16 rings = 64 front detectors

back detectors: 4 quadrants * 12 strips = 48 back detectors

but to do this, one need all the centroids of the peaks from both sides:

front: 64 detectors * 2 peaks/ring = 128 centroids

back: 48 detectors * 2 peaks/ring * 16 rings = 1536 centroids

total centroids to collect: 1664 centroids (this I did not want to do manually)

Full calibration with 16 rings and 12 back strips. We had to remove the innermost ring.

MOVE THE BELOW TO APPENDIX?

Tilbakemelding:

up to you. I would do like this:

very technical things about scripts etc. I would move to an appendix. If it helps understanding what you did, I would leave it in the text.

For each file converted with MedToRoot, the program makes four files; OffBeam, OnBeam, OnBeamBackground and Scaler. The file we are interested in for analysis is the OnBeam file.

First all of the interesting files are converted with the M2R.sh script.

```
$ cd /Users/trondwj/GitHub/MasterThesis/Scripts/sorting
$ ./M2R.sh Sm
```

Then the OnBeam files from M2R.sh is run through using Treebuilder in the AQ4S.sh script.

```
$ cd /Users/trondwj/GitHub/MasterThesis/Scripts/sorting
$ ./AQ4S.sh Sm user TB
$ mv Sm_user-TreeBuilder-2019-04-10.root ../../Sorted_data/
```

After the sorting, I moved the file to a folder of sorted data, and gave the relative path in the setup_Sm.txt file in Scripts/plotting/ used as input in the MultiPlot.cpp script. Using the MultiPlot.cpp script, the ADC time offsets can be extracted by the following commands

```
$ cd /Users/trondwj/GitHub/MasterThesis/Scripts/plotting
$ root
root [0] .L MultiPlot.cpp++
root [1] check_ADC_time_offsets("setup_Sm.txt")
```

or they can be manually reached by

```
$ cd /Users/trondwj/GitHub/MasterThesis/Sorted_data
$ root Sm_user-TreeBuilder-2019-04-10.root
root [1] new TBrowser()
```

and in the browser, the histograms named tdiff_gp_ *i* (where *i* is a number between 0 and 3) will lie under all the folders. The peaks of these plots have the interesting x-value. Zooming into the peaks, it is very clear what value it is. These values are provided in the calibration file under ADC time offsets (ticks). These values can change depending on the amount of data sorted, so it is wise to double check them.

After the peak values have been collected, they should be written into the calibration file

```
# ADC time offsets (ticks)
adc_0.TimeOffset: 0
adc_1.TimeOffset: -2
```

```
adc_2.TimeOffset: -3
adc_3.TimeOffset: 5
```

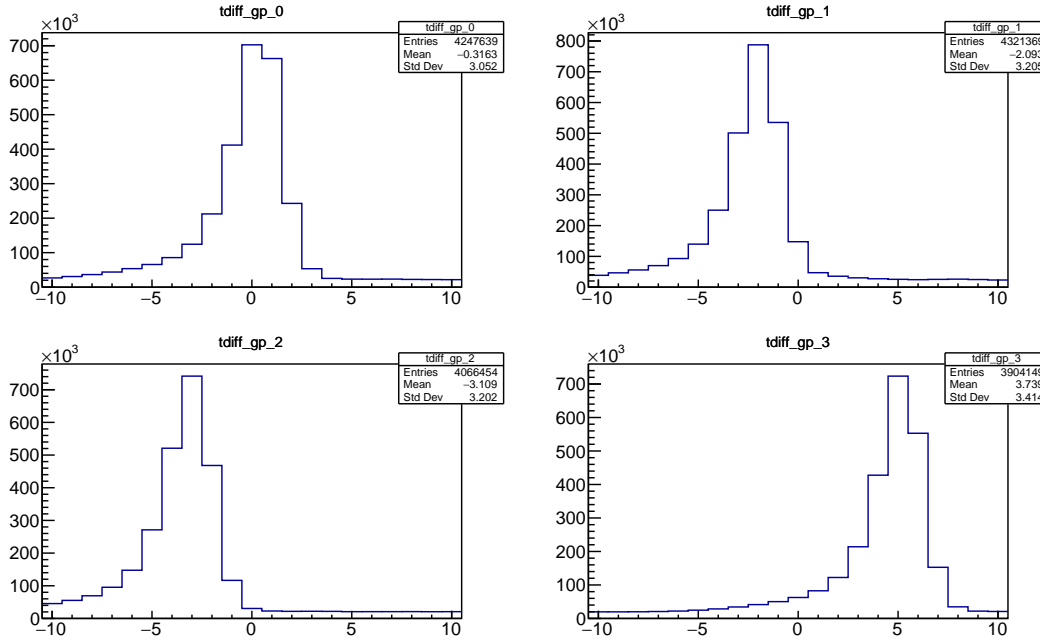


Figure 4.1: ADC time offsets.

Tilbakemelding:
one time spectrum per quadrant?

HUSK: Si noe om ADC time offsets + Threshold. Og at man må se på det tidlig, så resortere.

M2R.sh → AQ4S.sh → check time offset → threshold → AQ4_fit() → particle-calibration.py → ADC-generator.py → copy the calibration from the terminal and paste into calibration file

Tilbakemelding:
need to explain the time spectra: start - stop
purpose: align time spectra so that you can set a prompt time gate.
→ correlate γ -rays with particles.

Simulation fit → AQ4_fit() → particle-calibration.py → ADC-generator.py
→ copy the calibration from the terminal and paste into calibration file

Visualize plots using ROOT and the scripts.
Skriv om scriptene som er lagd, og at det var litt vanskelig å automatisere kalibreringen. Hvis det skulle vært gjort måtte vi funnet en funksjon med ”negatively skewed distribution” or ”negative skewness” (right modal), en ”left skewed function” (most data is more than the mean).

I log-skala ser dette mer Gaussisk ut, men det er ikke det i non-log skala.

Back detector calibration: There are just too much individual differences to calibrate the back detectors with a simple script given a range for all 12 back strips. I found out this way to late. There isn't any range to rule them all, at least since the fitting function can behave very strange given a too small or too big range.

— Mail from Liam begins —

"You might have to investigate the threshold a little bit. The continuum of events at low energy comes from charge sharing between the strips. For these very heavy ions, the total amount of charge deposited gets split between neighbouring strips of the CD. The code does performs some tricks to try and recover the correct energy and position, but that depends on counting the number of strips that fire. Therefore, if the threshold is too low you will include "pedestal" events and it will get things wrong. If the threshold is too high, you will miss some events that have charge sharing and get the wrong energy for your particle.

The key spectra to look at are "part" and "cd_debug". The latter counts how many particles have X strips fired on the front side and Y strips fired on the back side.

If you have too many cd_debug events = 3, then your thresholds are too low. If you have a large continuum/background in the "part" spectrum, your thresholds are too high. Best thing to do is play about with different values.

Bin 20 is when no particle can be found, because there is no energy registered in either the front or the back strips. This can only happen when the front energy is below the software threshold that you set and the back energy is either in a broken strip or is also below the software threshold. Likely it is some noise events or charge sharing that comes below the threshold.

The major problem with the online calibration is that a number of the back strips have the wrong gains, but it otherwise looks quite good. Have you identified which strips these are, by comparing the gains between the 'online' and 'user' calibrations? You could maybe correct those strips as an intermediate step and see how things look.

the source has a thickness of 1.23 mm, which needs to be factored in so that the CD to target distance is the CD to source distance PLUS the source thickness, i.e. $25.78 \text{ mm} + 1.23 \text{ mm} = 27.01 \text{ mm}$. This is very close to the 26.98 mm you got from us in August. I think that the source data was reanalyzed since the original blog entry, giving the 0.03 mm difference!"

For the centroids, it is very hard to tell in log scale how precise you are with the automatic fitting. I zoomed in on one example (attached) and you can see that the black lines do not really represent the centroid in this instance (black lines too low in energy). Because of the complex peak shapes, it is very hard to do this with automatic fitting it seems.

It honestly might be better to simply hover your mouse over the correct "feature" of the peak, be it the centroid or the maximum, and compare that.

The fitting just doesn't seem reliable.

If you do not have the cdpad option selected, then there will be no particle events, because they come in the CD. The -s flag is for adding particles which come without a gamma-ray and the add back flag is for adding Compton scattered events together in the Miniball clusters.

What you observe around channel number 20 in the ADC events is the so-called pedestal. There is a single common gate for each ADC (containing channels from one CD quadrant). Therefore, when there is an event in one strip of the CD all channels are readout, but the channels without a real event read a "zero" energy. These are the events in the pedestal. You should define your threshold for each ADC channel to be above this peak. You are simply zoomed in to the wrong range. Maybe try with log scale on the y-axis and you will see that there should be a cut off at low-energy. After a correct calibration is applied (as you can see for adc_1_19 in your example), this pedestal will be calibrated out of the physical energy range.

The nominal calibration will be quite good for most detectors in a certain energy range, because it is designed to be that way. The gains of each DGF are matched during the setup of the experiment so that the online analysis is more straightforward. However, there are some non-linearities and drifting offsets and gains over time that have to be corrected for with a proper calibration using the $^{133}\text{Ba}/^{152}\text{Eu}$ source data.

— Mail from Liam ended —

Tilbakemelding:

I presume that charge sharing is only considered if 2 firing strips are neighbors?

Pedestal

The pedestal is like a massive statue in front of the interesting data.

We use a threshold to cut away the pedestal.

Threshold

* Threshold (forskjellig i log/ikke-log skala)

Using a logarithmic y-axis, the threshold value will decrease very much. So don't use that.

Tilbakemelding:

easier to set thresholds on lin. scale.

Threshold: The code has a default threshold of 100, but in some cases this is too much and some cases this is not enough. So for each adc channel, the threshold can be set. We don't want to include the "pedestal". Charge sharing. Won't cut too much or too little..

CD debug:

```
$ cd /Users/trondwj/GitHub/MasterThesis/Scripts/plotting
$ root
root [0] .L MultiPlot.cpp++
root [1] check_cd_debug("setup_Sm.txt")
```

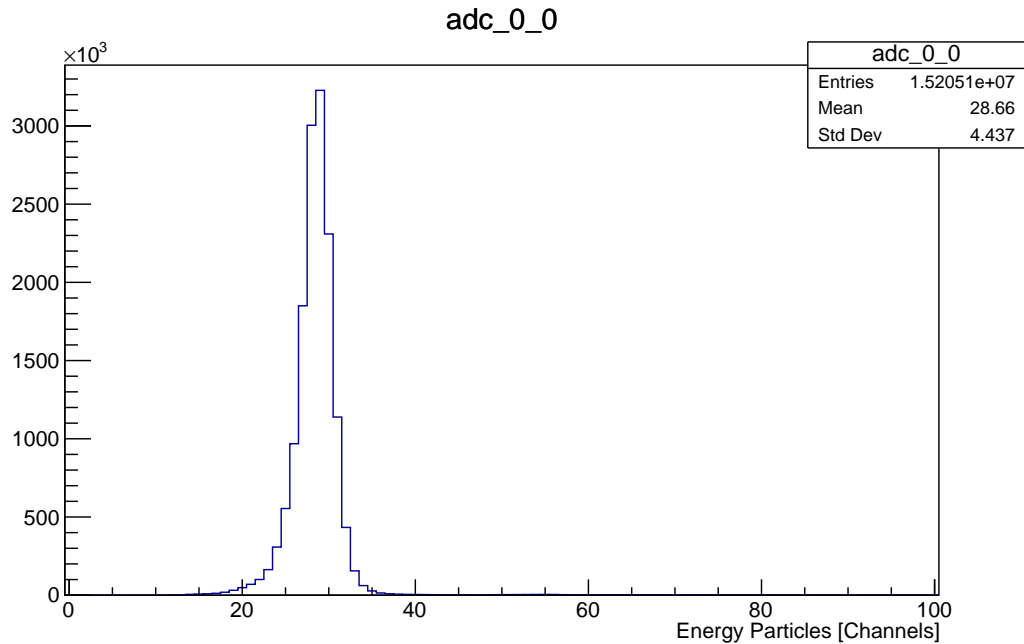


Figure 4.2: Pedestal Q1, f1.

4.4.1 Particle detector

User calibration

ADC: Analog to digital converter (Mesytec)

TDC: Time to digital converter

DSSSD: Double-Sided Silicon Strip Detector \Rightarrow CD

must remove the inner ring from data analysis because of damage

$$\text{gain} = \frac{E_{\text{Sm}} - E_{\text{Pb}}}{Ch_{\text{Sm}} - Ch_{\text{Pb}}}$$

$$\text{offset} = E_{\text{Sm}} - \text{gain} \cdot Ch_{\text{Sm}}$$

in keV.

Hvis man har flere sentroider bruker man bare lineær regresjon. Gjelder spesielt for baksiden!

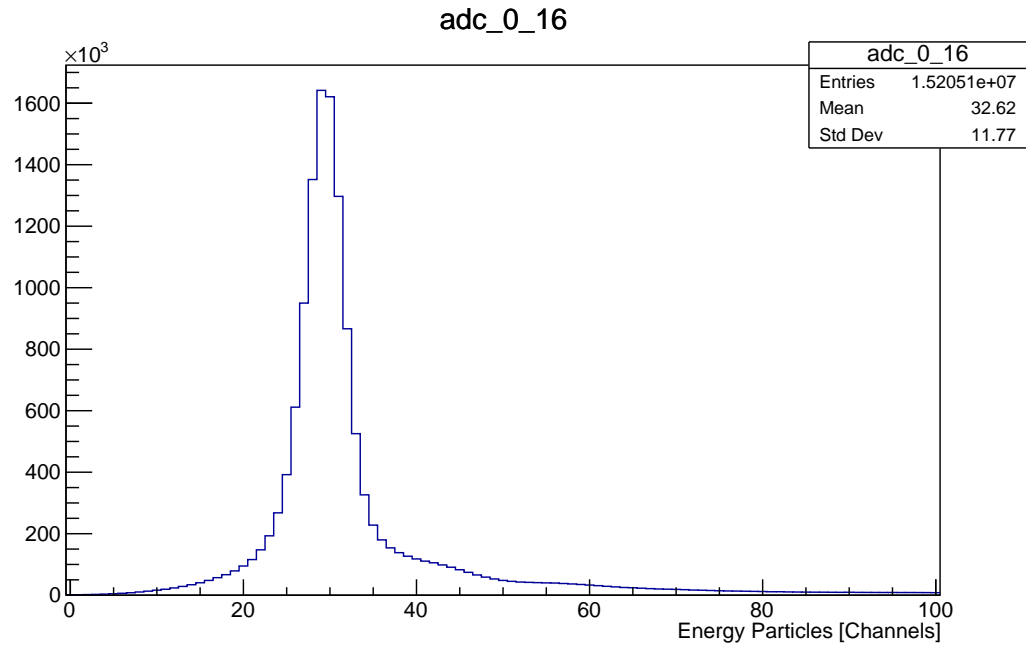


Figure 4.3: Pedestal Q1, b1.

Online calibration

4.4.2 Gamma detectors

DGF: Digital γ finder
addback, singles, ...

4.5 Doppler correction

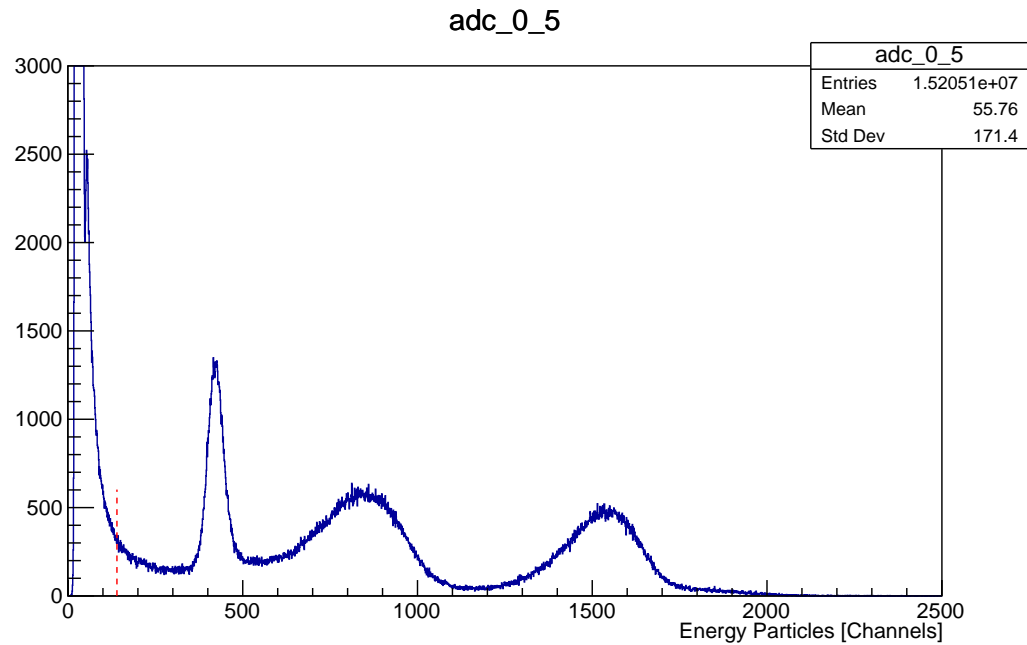


Figure 4.4: Threshold Q1, f6.

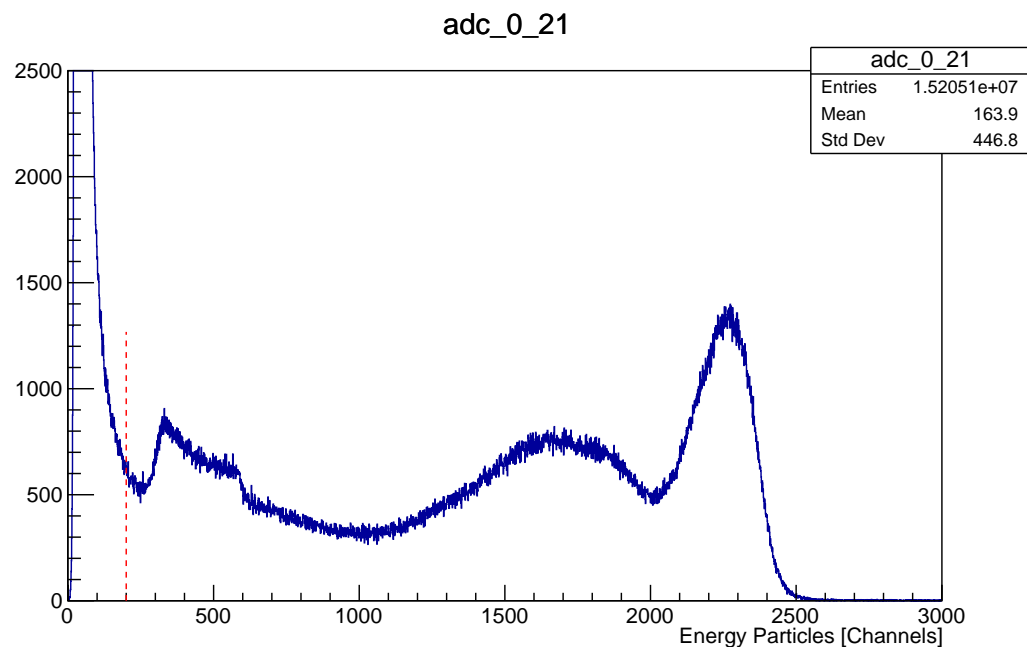


Figure 4.5: Threshold Q1, b6.

Table 4.3: TreeBuilder vs AQ4Sort.

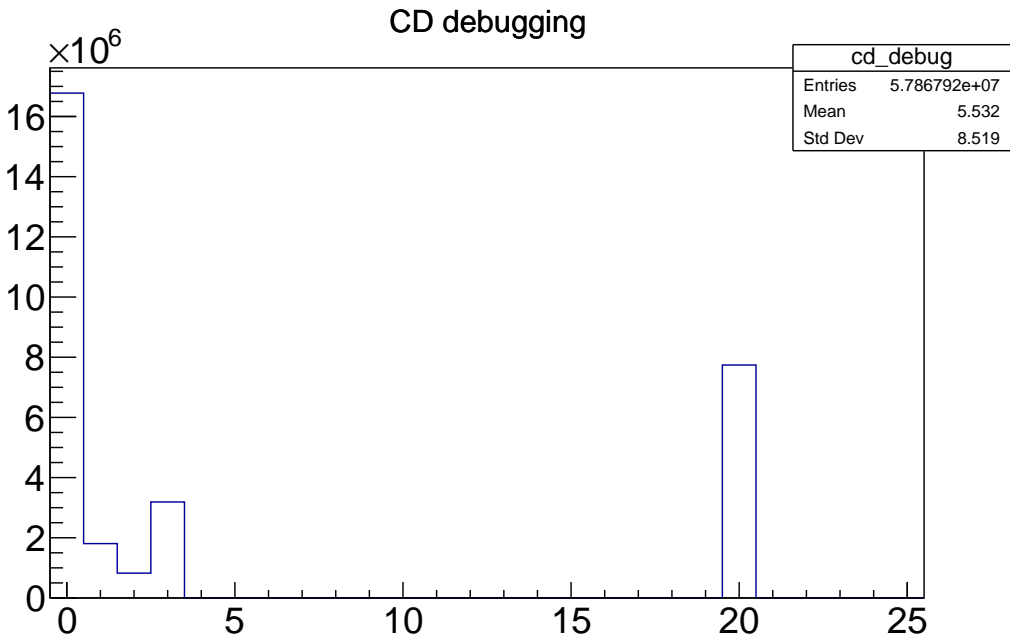
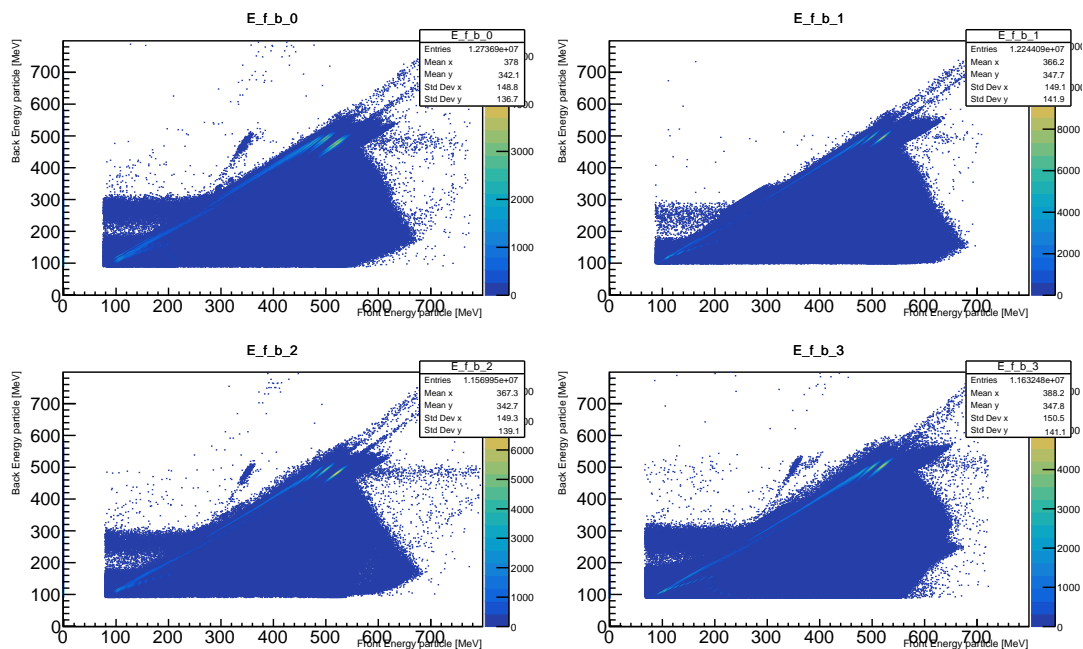
Quadrant	Front ring [F] or back strip [B]	TreeBuilder	AQ4Sort
1	F 15	adc_0_0	fE_Q1_f1
1	F 14	adc_0_1	fE_Q1_f2
1	F 13	adc_0_2	fE_Q1_f3
:	:	:	:
1	F 1	adc_0_14	fE_Q1_f15
1	F 0	adc_0_15	fE_Q1_f16
1	B 0	adc_0_16	bE_Q1_f1
1	B 1	adc_0_17	bE_Q1_f2
1	B 2	adc_0_18	bE_Q1_f3
:	:	:	:
1	B 11	adc_0_26	bE_Q1_f11
1	B 12	adc_0_27	bE_Q1_f12
2	F 15	adc_1_0	fE_Q2_f1
:	:	:	:
2	F 0	adc_1_15	fE_Q2_f16
2	B 0	adc_1_16	bE_Q2_f1
:	:	:	:
2	B 12	adc_1_27	bE_Q2_f12
3	F 15	adc_2_0	fE_Q3_f1
:	:	:	:
3	F 0	adc_2_15	fE_Q3_f16
3	B 0	adc_2_16	bE_Q3_f1
:	:	:	:
3	B 12	adc_2_27	bE_Q3_f12
4	F 15	adc_3_0	fE_Q4_f1
:	:	:	:
4	F 0	adc_3_15	fE_Q4_f16
4	B 0	adc_3_16	bE_Q4_f1
:	:	:	:
4	B 12	adc_3_27	bE_Q4_f12

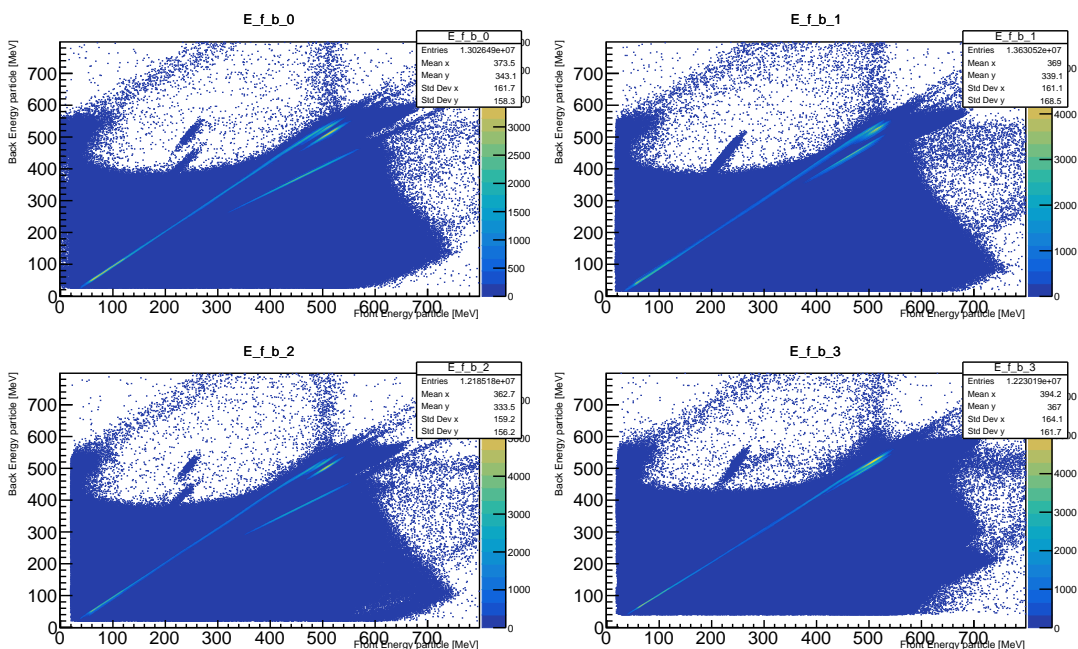
Table 4.4: ADC

ADC	Quadrant	Channel	Front ring [F] or back strip [B]
0 - 3	1 - 4	0	F
0 - 3	1 - 4	1	F
0 - 3	1 - 4	2	F
0 - 3	1 - 4	3	F
0 - 3	1 - 4	4	F
0 - 3	1 - 4	5	F
0 - 3	1 - 4	6	F
0 - 3	1 - 4	7	F
0 - 3	1 - 4	8	F
0 - 3	1 - 4	9	F
0 - 3	1 - 4	10	F
0 - 3	1 - 4	11	F
0 - 3	1 - 4	12	F
0 - 3	1 - 4	13	F
0 - 3	1 - 4	14	F
0 - 3	1 - 4	15	F
0 - 3	1 - 4	16	B
0 - 3	1 - 4	17	B
0 - 3	1 - 4	18	B
0 - 3	1 - 4	19	B
0 - 3	1 - 4	20	B
0 - 3	1 - 4	21	B
0 - 3	1 - 4	22	B
0 - 3	1 - 4	23	B
0 - 3	1 - 4	24	B
0 - 3	1 - 4	25	B
0 - 3	1 - 4	26	B
0 - 3	1 - 4	27	B
0 - 3		28	Empty
0 - 3		29	Empty
0 - 3		30	Empty
0 - 3	1 - 4	31	PAD
4		0	Ionization Chamber
4		1	Ionization Chamber

Table 4.5: DGF

Cluster	Segment	Channel	Name
0 - 3	1 - 4	0	

**Figure 4.6:** CD debugging.**Figure 4.7:** User calibration.

**Figure 4.8:** Online calibration.

Chapter 5

Experimental results

Very pure beam (did we have statistics of this?) - resultat til avhandling. sjekk etter doppler-korrigering. Nd-contaminasjon? i så fall veldig lite, 1-2 prosent?

Tilbakemelding:

we would have to look at the γ -spectra to identify any contaminants. There may be a little bit of Nd-140 in the beam, but if so, it is very little (judging from on-line spectra).

Chapter 6

Discussion

Level scheme (from Klintefjord?)

Tilbakemelding:

at some point you should show the level scheme.

- motivation: to explain what is known, and which transition probabilities you want to measure.

Perhaps also to explain what theory predicts.

- discussion: if you get γ -spectrum for $^{140}\text{Sm} \rightarrow$ to explain what you see.

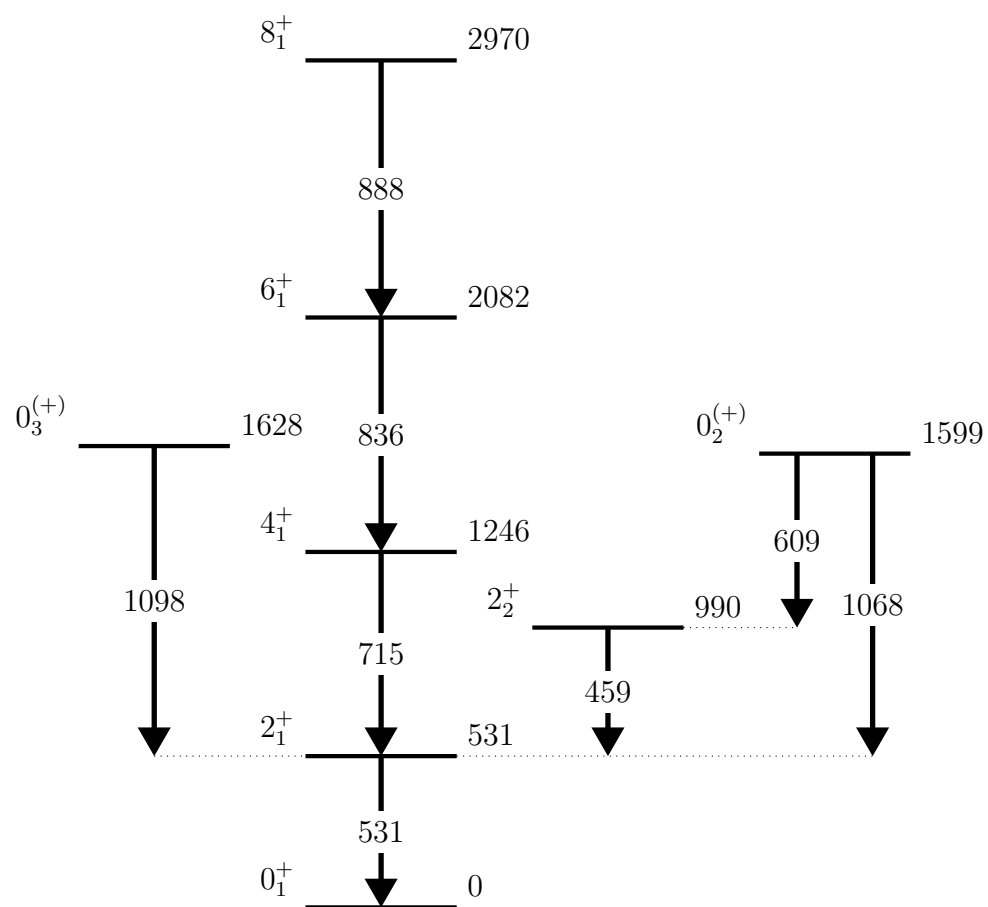


Figure 6.1: Level scheme for ^{140}Sm . Adapted from Klintefjord.

Chapter 7

Summary and outlook

Future work: Better calibration of particle detectors (online not perfect). Take into account the shape of the peaks \Rightarrow calibrate the particle detectors manually.. Takes a lot of time! But maybe less than trying to fit all in a script? Had I just known...

Fra oppgaveteksten:

determine Coulomb excitation yields. These yields will then, in a second step, be compared to theoretical calculations and transition probabilities and quadrupole moments will be extracted using chi-square minimization procedures.

GOSIA and GOSIA2 analysis?

https://www.pas.rochester.edu/~cline/Gosia/Gosia_Manual_20110609.pdf

Appendices

Appendix A

Symbol list

Table A.1: Table of symbols with explanations.

T _{1/2}	Half-life
------------------	-----------

Appendix B

Acronyms and abbreviations

Table B.1: Table of acronyms and abbreviations.

ADC	Analog to Digital Converter
CERN	European Council for Nuclear Research (in French: Conseil Européen pour la Recherche Nucléaire)
CD	Compact Disc
COULEX	COULomb EXcitation
DAQ	Data AcQuisition
DGF	Digital Gamma Finder
DSSSD	Double Sided Silicon Strip Detector (also known as CD)
GPS	General Purpose Separator
HRS	High Resolution Separator
HIE-ISOLDE	High Intensity and Energy upgrade at ISOLDE
HPGe	High Purity Germanium
ISOL	Isotope Separator On Line
ISOLDE	ISOL DEvice
LINAC	LINear ACcelerator
MBS	Multi Branch System
MED	MBS Event Data (also known as Miniball Event Data)
MAR _a BQU	MBS And ROOT Based Online/Offline Utility
PSB	Proton Synchrotron Booster
REX	Radioactive beam EXperiment
EBIS	Electron Beam Ion Source
REXEgis	Radioactive beam EXperiment Electron Beam Ion Source
REXTRAP	Radioactive beam EXperiment TRAP
REX-ISOLDE	Radioactive beam EXperiment at ISOLDE
RIB	Radioactive Ion Beam
RILIS	Resonance Ionization Laser Ion Source
TDC	Time to Digital Converter

Appendix C

Two-particle collision

C.1 Laboratory (LAB) frame of reference

The angles of the two-particle collision in the laboratory frame from [Figure 3.8a](#) is calculated in this section. A general approach is used to make it easier to hold track of the parameters. From the figure we can express the velocities as

$$\begin{aligned}\mathbf{u} &= \mathbf{u}_1 = u\hat{\mathbf{x}} \\ \mathbf{u}_2 &= 0 \\ \mathbf{v}_b &= \mathbf{v}_1 = v_1(\cos\theta\hat{\mathbf{x}} + \sin\theta\hat{\mathbf{y}}) \\ \mathbf{v}_t &= \mathbf{v}_2 = v_2(\cos\varphi\hat{\mathbf{x}} - \sin\varphi\hat{\mathbf{y}})\end{aligned}\tag{C.1}$$

where \mathbf{u}_1 and \mathbf{v}_1 is the initial and final velocity of the projectile $m_b = m_1$ respectively, and \mathbf{u}_2 and \mathbf{v}_2 is the initial and final velocity of the target $m_t = m_2$ respectively. The angles $\theta_b = \theta$ and $\theta_t = \varphi$ are the projectile and target angle respectively. We also introduce a ratio of the projectile mass to the target mass, $\alpha = m_1/m_2$.

Conservation of momentum gives

$$m_1\mathbf{u}_1 = m_1\mathbf{v}_1 + m_2\mathbf{v}_2$$

which in x-direction can be expressed as

$$\begin{aligned}m_1u &= m_1v_1 \cos\theta + m_2v_2 \cos\varphi \\ m_1(u - v_1 \cos\theta) &= m_2v_2 \cos\varphi \\ \frac{m_1}{m_2}(u - v_1 \cos\theta) &= v_2 \cos\varphi \\ \alpha(u - v_1 \cos\theta) &= v_2 \cos\varphi\end{aligned}\tag{C.2}$$

and in y-direction can be expressed as

$$\begin{aligned} 0 &= m_1 v_1 \sin \theta - m_2 v_2 \sin \varphi \\ m_1 v_1 \sin \theta &= m_2 v_2 \sin \varphi \\ \frac{m_1}{m_2} v_1 \sin \theta &= v_2 \sin \varphi \\ \alpha v_1 \sin \theta &= v_2 \sin \varphi \end{aligned} \quad (\text{C.3})$$

Conservation of energy gives

$$\begin{aligned} \frac{1}{2} m_1 \mathbf{u}_1^2 &= \frac{1}{2} m_1 \mathbf{v}_1^2 + \frac{1}{2} m_2 \mathbf{v}_2^2 \\ \frac{1}{2} m_1 (u^2 - v_1^2) &= \frac{1}{2} m_2 v_2^2 \\ \frac{m_1}{m_2} (u^2 - v_1^2) &= v_2^2 \\ \alpha (u^2 - v_1^2) &= v_2^2 \end{aligned} \quad (\text{C.4})$$

We now have three equations (Equation (C.2) - Equation (C.4)) with four unknown quantities ($v_1, \theta, v_2, \varphi$). Using the target angle φ as an independent variable, we can find expressions for the other three variables.

Squaring Equation (C.2)

$$\begin{aligned} \alpha^2 (u - v_1 \cos \theta)^2 &= v_2^2 \cos^2 \varphi \\ \alpha^2 (u^2 - 2uv_1 \cos \theta + v_1^2 \cos^2 \theta) &= v_2^2 \cos^2 \varphi \end{aligned}$$

and Equation (C.3)

$$\alpha^2 v_1^2 \sin^2 \theta = v_2^2 \sin^2 \varphi$$

and adding them together gives

$$\begin{aligned} \alpha^2 (u^2 - 2uv_1 \cos \theta + v_1^2 \cos^2 \theta + v_1^2 \sin^2 \theta) &= v_2^2 (\cos^2 \varphi + \sin^2 \varphi) \\ \alpha^2 (u^2 - 2uv_1 \cos \theta + v_1^2) &= v_2^2 \\ \alpha^2 u^2 - 2\alpha^2 uv_1 \cos \theta + \alpha^2 v_1^2 &= v_2^2 \\ \alpha^2 v_1^2 &= -\alpha^2 u^2 + 2\alpha^2 uv_1 \cos \theta + v_2^2 \\ \alpha^2 v_1^2 &= -\alpha^2 u^2 + 2\alpha u (\alpha v_1 \cos \theta) + v_2^2 \end{aligned} \quad (\text{C.5})$$

From Equation (C.2) we have

$$\begin{aligned} \alpha(u - v_1 \cos \theta) &= v_2 \cos \varphi \\ \alpha u - \alpha v_1 \cos \theta &= v_2 \cos \varphi \\ \alpha v_1 \cos \theta &= \alpha u - v_2 \cos \varphi \end{aligned} \quad (\text{C.6})$$

Substituting for [Equation \(C.6\)](#) into [Equation \(C.5\)](#) we get

$$\begin{aligned}\alpha^2 v_1^2 &= -\alpha^2 u^2 + 2\alpha u(\alpha u - v_2 \cos \varphi) + v_2^2 \\ \alpha^2 v_1^2 &= -\alpha^2 u^2 + 2\alpha^2 u^2 - 2\alpha u v_2 \cos \varphi + v_2^2 \\ \alpha^2 v_1^2 &= \alpha^2 u^2 - 2\alpha u v_2 \cos \varphi + v_2^2\end{aligned}\quad (\text{C.7})$$

Using [Equation \(C.4\)](#) we get

$$\begin{aligned}\left(\frac{\alpha}{\alpha}\right) \alpha(u^2 - v_1^2) &= v_2^2 \\ \alpha^2(u^2 - v_1^2) &= \alpha v_2^2 \\ \alpha^2 u^2 - \alpha^2 v_1^2 &= \alpha v_2^2 \\ \alpha^2 v_1^2 &= \alpha^2 u^2 - \alpha v_2^2\end{aligned}\quad (\text{C.8})$$

Combining [Equation \(C.7\)](#) and [Equation \(C.8\)](#) gives

$$\begin{aligned}\alpha^2 u^2 - 2\alpha u v_2 \cos \varphi + v_2^2 &= \alpha^2 u^2 - \alpha v_2^2 \\ v_2^2 + \alpha v_2^2 &= 2\alpha u v_2 \cos \varphi \\ v_2^2(1 + \alpha) &= 2\alpha u v_2 \cos \varphi \\ v_2 &= 2 \left(\frac{\alpha}{1 + \alpha} \right) u \cos \varphi\end{aligned}\quad (\text{C.9})$$

Substituting [Equation \(C.9\)](#) into [Equation \(C.8\)](#) we get

$$\begin{aligned}\alpha^2 v_1^2 &= \alpha^2 u^2 - \alpha \left(2 \left(\frac{\alpha}{1 + \alpha} \right) u \cos \varphi \right)^2 \\ v_1^2 &= u^2 - \frac{1}{\alpha} \left(4 \left(\frac{\alpha^2}{(1 + \alpha)^2} \right) u^2 \cos^2 \varphi \right) \\ v_1^2 &= u^2 \left(1 - 4 \left(\frac{\alpha}{(1 + \alpha)^2} \right) \cos^2 \varphi \right) \\ v_1 &= u \sqrt{1 - 4 \frac{\alpha}{M} \cos^2 \varphi}\end{aligned}\quad (\text{C.10})$$

where $\alpha/M = \alpha/(1 + \alpha)^2$. The ratio of [Equation \(C.3\)](#) and [Equation \(C.6\)](#) gives

$$\begin{aligned}\frac{\alpha v_1 \sin \theta}{\alpha v_1 \cos \theta} &= \frac{v_2 \sin \varphi}{\alpha u - v_2 \cos \varphi} \\ \tan \theta &= \frac{v_2 \sin \varphi}{\alpha u - v_2 \cos \varphi}\end{aligned}\quad (\text{C.11})$$

Inserting Equation (C.9) into Equation (C.11) gives

$$\begin{aligned}
 \tan \theta &= \frac{\left(2\left(\frac{\alpha}{1+\alpha}\right) u \cos \varphi\right) \sin \varphi}{\alpha u - \left(2\left(\frac{\alpha}{1+\alpha}\right) u \cos \varphi\right) \cos \varphi} \\
 \tan \theta &= \frac{\alpha u \left(\frac{1}{1+\alpha}\right) 2 \sin \varphi \cos \varphi}{\alpha u \left(1 - 2\left(\frac{1}{1+\alpha}\right) \cos^2 \varphi\right)} \\
 \tan \theta &= \frac{\sin 2\varphi}{\left(1 + \alpha\right) \left(1 - 2\left(\frac{1}{1+\alpha}\right) \cos^2 \varphi\right)} \\
 \tan \theta &= \frac{\sin 2\varphi}{1 + \alpha - 2 \cos^2 \varphi} \\
 \tan \theta &= \frac{\sin 2\varphi}{\alpha - (2 \cos^2 \varphi - 1)} \\
 \tan \theta &= \frac{\sin 2\varphi}{\alpha - \cos 2\varphi} \\
 \theta &= \arctan \left(\frac{\sin 2\varphi}{\alpha - \cos 2\varphi} \right)
 \end{aligned} \tag{C.12}$$

Substituting back the variable names from Figure 3.8a into Equation (C.12) gives

$$\theta_b = \arctan \left(\frac{\sin 2\theta_t}{\alpha - \cos 2\theta_t} \right) \tag{C.13}$$

C.2 Center of mass (CM) frame of reference

Using the same approach as section C.1. From figure Figure 3.8b we can express the velocities as

$$\begin{aligned}
 \mathbf{u}'_1 &= u'_1 \hat{\mathbf{x}} \\
 \mathbf{u}'_2 &= u'_2 \hat{\mathbf{x}} \\
 \mathbf{v}'_b &= \mathbf{v}'_1 = v'_1 (\cos \theta' \hat{\mathbf{x}} + \sin \theta' \hat{\mathbf{y}}) \\
 \mathbf{v}'_t &= \mathbf{v}'_2 = v'_2 (-\cos \theta' \hat{\mathbf{x}} - \sin \theta' \hat{\mathbf{y}}) = -v'_2 (\cos \theta' \hat{\mathbf{x}} + \sin \theta' \hat{\mathbf{y}})
 \end{aligned} \tag{C.14}$$

where \mathbf{u}'_1 and \mathbf{v}'_1 is the initial and final velocity of the projectile $m_b = m_1$ respectively, and \mathbf{u}'_2 and \mathbf{v}'_2 is the initial and final velocity of the target $m_t = m_2$ respectively. The angle $\theta'_b = \theta'$ is the projectile angle.

In the center of mass (CM) frame of reference, the position of the center of mass is given by

$$\mathbf{R} = \frac{m_1 \mathbf{r}_1 + m_2 \mathbf{r}_2}{m_1 + m_2} \tag{C.15}$$

and the velocity is

$$\mathbf{V} = \frac{d\mathbf{R}}{dt} = \frac{d}{dt} \left(\frac{m_1 \mathbf{r}_1 + m_2 \mathbf{r}_2}{m_1 + m_2} \right) = \frac{m_1 \mathbf{u}'_1 + m_2 \mathbf{u}'_2}{m_1 + m_2} \quad (\text{C.16})$$

At the origin of the CM frame, $\mathbf{R} = 0$, which implies $\mathbf{V} = 0$. The total momentum before the collision is

$$\begin{aligned} m_1 \mathbf{u}'_1 + m_2 \mathbf{u}'_2 &= 0 \\ m_2 \mathbf{u}'_2 &= -m_1 \mathbf{u}'_1 \\ \mathbf{u}'_2 &= -\frac{m_1}{m_2} \mathbf{u}'_1 \\ \mathbf{u}'_2 &= -\alpha \mathbf{u}'_1 \end{aligned} \quad (\text{C.17})$$

and after the collision it is

$$\begin{aligned} m_1 \mathbf{v}'_1 + m_2 \mathbf{v}'_2 &= 0 \\ m_2 \mathbf{v}'_2 &= -m_1 \mathbf{v}'_1 \\ \mathbf{v}'_2 &= -\frac{m_1}{m_2} \mathbf{v}'_1 \\ \mathbf{v}'_2 &= -\alpha \mathbf{v}'_1 \\ -v'_2 (\cos \theta' \hat{\mathbf{x}} + \sin \theta' \hat{\mathbf{y}}) &= -\alpha v'_1 (\cos \theta' \hat{\mathbf{x}} + \sin \theta' \hat{\mathbf{y}}) \\ v'_2 &= \alpha v'_1 \end{aligned} \quad (\text{C.18})$$

Conservation of energy gives

$$\begin{aligned} \frac{1}{2} m_1 u'^2_1 + \frac{1}{2} m_2 u'^2_2 &= \frac{1}{2} m_1 v'^2_1 + \frac{1}{2} m_2 v'^2_2 \\ m_1 u'^2_1 + m_2 u'^2_2 &= m_1 v'^2_1 + m_2 v'^2_2 \end{aligned} \quad (\text{C.19})$$

Substituting Equation (C.17) and Equation (C.18) into Equation (C.19) gives

$$\begin{aligned} m_1 u'^2_1 + m_2 (-\alpha u'_1)^2 &= m_1 v'^2_1 + m_2 (\alpha v'_1)^2 \\ m_1 u'^2_1 + \alpha^2 m_2 u'^2_1 &= m_1 v'^2_1 + \alpha^2 m_2 v'^2_1 \\ (m_1 + \alpha^2 m_2) u'^2_1 &= (m_1 + \alpha^2 m_2) v'^2_1 \\ u'^2_1 &= v'^2_1 \\ u'_1 &= v'_1 \end{aligned} \quad (\text{C.20})$$

Substituting Equation (C.20) into Equation (C.17) gives

$$u'_2 = -\alpha v'_1 \quad (\text{C.21})$$

C.3 Connection between the LAB frame and the CM frame

Galilean transformations describes the relationship between the LAB frame and the CM frame

$$\begin{aligned} x' &= x - vt & v'_x &= v_x - V_{cm} \\ y' &= y & v'_y &= v_y \\ z' &= z & v'_z &= v_z \\ t' &= t \end{aligned}$$

Using the same approach as section C.1. In the LAB frame Figure 3.8a, conservation of momentum is given by

$$m_1 \mathbf{u}_1 + m_2 \mathbf{u}_2 = m_1 \mathbf{v}_1 + m_2 \mathbf{v}_2 = (m_1 + m_2) \mathbf{V} \quad (\text{C.22})$$

which can be written as

$$\begin{aligned} m_1 \mathbf{u}_1 + m_2 \mathbf{u}_2 &= (m_1 + m_2) \mathbf{V} \\ \mathbf{V} &= \frac{m_1 \mathbf{u}_1 + m_2 \mathbf{u}_2}{m_1 + m_2} & \mathbf{u}_2 &= 0 \\ \mathbf{V} &= \frac{m_1}{m_1 + m_2} \mathbf{u}_1 \\ \mathbf{V} &= \frac{\alpha}{1 + \alpha} u \hat{\mathbf{x}} \\ V &= \frac{\alpha}{1 + \alpha} u \end{aligned} \quad (\text{C.23})$$

Using Galilean transformations, the connection between \mathbf{v}'_1 and \mathbf{v}_1 is expressed as

$$\begin{aligned} \mathbf{v}'_1 &= \mathbf{v}_1 - \mathbf{V} \\ \mathbf{v}_1 &= \mathbf{v}'_1 + \mathbf{V} \end{aligned} \quad (\text{C.24})$$

which in x-direction gives

$$v_1 \cos \theta = v'_1 \cos \theta' + V \quad (\text{C.25})$$

and in y-direction gives

$$v_1 \sin \theta = v'_1 \sin \theta' \quad (\text{C.26})$$

The ratio of [Equation \(C.26\)](#) and [Equation \(C.25\)](#) gives

$$\begin{aligned}\frac{v_1 \sin \theta}{v_1 \cos \theta} &= \frac{v'_1 \sin \theta'}{v'_1 \cos \theta' + V} \\ \tan \theta &= \frac{\sin \theta'}{\cos \theta' + \frac{V}{v'_1}} \\ \tan \theta &= \frac{\sin \theta'}{\frac{V}{v'_1} + \cos \theta'}\end{aligned}\tag{C.27}$$

We need to reformulate the velocity ratio. Substitution from [Equation \(C.20\)](#) gives

$$\frac{V}{v'_1} = \frac{V}{u'_1}\tag{C.28}$$

Using Galilean transformation and [Equation \(C.23\)](#) we have that

$$\begin{aligned}\mathbf{u}'_1 &= \mathbf{u}_1 - \mathbf{V} \\ u'_1 &= u_1 - V \\ u'_1 &= u - \frac{\alpha}{1+\alpha}u \\ u'_1 &= u \left(1 - \frac{\alpha}{1+\alpha}\right) \\ u'_1 &= u \left(\frac{1+\alpha-\alpha}{1+\alpha}\right) \\ u'_1 &= \frac{1}{1+\alpha}u\end{aligned}\tag{C.29}$$

Substituting [Equation \(C.23\)](#) and [Equation \(C.29\)](#) into [Equation \(C.28\)](#) gives

$$\frac{V}{u'_1} = \frac{\frac{\alpha}{1+\alpha}u}{\frac{1}{1+\alpha}u} = \alpha\tag{C.30}$$

Substituting [Equation \(C.30\)](#) into [Equation \(C.27\)](#) gives

$$\begin{aligned}\tan \theta &= \frac{\sin \theta'}{\alpha + \cos \theta'} \\ \theta &= \arctan \left(\frac{\sin \theta'}{\alpha + \cos \theta'} \right)\end{aligned}\tag{C.31}$$

Substituting back the variable names from [Figure 3.8b](#) into [Equation \(C.31\)](#) gives

$$\theta_b = \arctan \left(\frac{\sin \theta'_b}{\alpha + \cos \theta'_b} \right) \quad (\text{C.32})$$

Using Galilean transformations, the connection between \mathbf{v}'_2 and \mathbf{v}_2 is expressed as

$$\begin{aligned} \mathbf{v}'_2 &= \mathbf{v}_2 - \mathbf{V} \\ \mathbf{v}_2 &= \mathbf{v}'_2 + \mathbf{V} \end{aligned} \quad (\text{C.33})$$

which in x-direction gives

$$\begin{aligned} v_2 \cos \varphi &= -v'_2 \cos \theta' + V \\ v_2 \cos \varphi &= V - v'_2 \cos \theta' \end{aligned} \quad (\text{C.34})$$

and in y-direction gives

$$v_2 \sin \varphi = v'_2 \sin \theta' \quad (\text{C.35})$$

The ratio of [Equation \(C.35\)](#) and [Equation \(C.34\)](#) gives

$$\begin{aligned} \frac{v_2 \sin \varphi}{v_2 \cos \varphi} &= \frac{v'_2 \sin \theta'}{V - v'_2 \cos \theta'} \\ \tan \varphi &= \frac{\sin \theta'}{\frac{V}{v'_2} - \cos \theta'} \end{aligned} \quad (\text{C.36})$$

We need to reformulate the velocity ratio. Substitution from [Equation \(C.18\)](#) and [Equation \(C.20\)](#) gives

$$\frac{V}{v'_2} = \frac{V}{\alpha v'_1} = \frac{V}{\alpha u'_1} \quad (\text{C.37})$$

Substituting [Equation \(C.30\)](#) into [Equation \(C.37\)](#) gives

$$\frac{V}{v'_2} = \frac{V}{\alpha \frac{V}{\alpha}} = 1 \quad (\text{C.38})$$

Substituting [Equation \(C.38\)](#) into [Equation \(C.36\)](#) gives

$$\begin{aligned}\tan \varphi &= \frac{\sin \theta'}{1 - \cos \theta'} = \frac{1}{\frac{1-\cos \theta'}{\sin \theta'}} = \frac{1}{\tan \frac{\theta'}{2}} = \cot \frac{\theta'}{2} \\ \varphi &= \frac{1}{2}(\pi - \theta') \text{ [radians]} = \frac{1}{2}(180^\circ - \theta') \text{ [degrees]}\end{aligned}\quad (\text{C.39})$$

Substituting back the variable names from [Figure 3.8](#) into [Equation \(C.39\)](#) gives

$$\theta_t = \frac{1}{2}(\pi - \theta'_b) \text{ [radians]} = \frac{1}{2}(180^\circ - \theta'_b) \text{ [degrees]} \quad (\text{C.40})$$

Appendix D

Source code

The sorting and analysis code used in this thesis has been developed at CERN-ISOLDE and can be found at <https://github.com/Miniball/MiniballCoulexSort>

The code for theoretical predictions of energy used in the calibration was developed by Liam Gaffney who is working at ISOLDE and has to do with analysis of data from Miniball and ISS. kinsim can be found here <https://github.com/lpgaff/kinsim>

Some calibration code is based on the codes of Ville Virtanen and Liam Gaffney.

Other code/scripts have been written by the author. C++ / Python.

Table D.1: Table of source code.

Name/Link	Description
MiniballCoulexSort	Sorting and analysis code
	Kinematic simulation

Appendix E

Connecting MiniballCoulexSort with ROOT

To connect MiniballCoulexSort with ROOT you need them to share their libraries with each other. This is done with a dynamic loader. You can find out more here: <https://root.cern.ch/root/html/doc/guides/users-guide/ROOTUsersGuide.html#file-system.rootrc>.

You have to make a `.rootrc` file in your home folder on your computer. In the `.rootrc` file you want to write something like this

```
Unix .*. Root .DynamicPath:    .:/Users/trondwj/GitHub(ROOT-
framework/build/lib >:/Users/trondwj/GitHub/Miniball/
MiniballCoulexSort/lib :
```

This should all be in one line. The first part is to tell the system to use the dynamic loader of ROOT to connect the given paths that follow. In my case the lib folder of the ROOT install was at

```
/Users/trondwj/GitHub(ROOT-framework/build/lib
```

and the lib folder of the MiniballCoulexSort was at

```
/Users/trondwj/GitHub/Miniball/MiniballCoulexSort/lib
```

These paths is totally individual, and you will probably not have it in the same place. Therefore these paths must be changed to fit your system.

After making the file you either have restart the terminal or you can source the file by writing this in the terminal

```
$ source ~/.rootrc
```


Appendix F

Running ROOT and MiniballCoulexSort from anywhere in the terminal

To run ROOT or the different scripts of MiniballCoulexSort anywhere in the terminal, you have to edit your `.bash_profile` file [.bash_profile on MacOS, .bashrc on Linux]. In my `.bash_profile` I used this

```
# Run ROOT from anywhere
export ROOTSYS=$HOME/GitHub(ROOT-framework/build
export PATH=$ROOTSYS/lib:$PATH
export PATH=$ROOTSYS/bin:$PATH
export DYLD_LIBRARY_PATH=$ROOTSYS/lib:$DYLD_LIBRARY_PATH

# Run MiniballCoulexSort from anywhere
export DYLD_LIBRARY_PATH=$HOME/GitHub/Miniball/
    MiniballCoulexSort/lib:$DYLD_LIBRARY_PATH
export PATH=$HOME/GitHub/Miniball/MiniballCoulexSort/lib:$PATH
export PATH=$HOME/GitHub/Miniball/MiniballCoulexSort/bin:$PATH
```

The DYLD_LIBRARY_PATH is used on Mac only. On other systems, use LD_LIBRARY_PATH. You need to locate the lib and bin folders for both ROOT and MiniballCoulexSort and change them to fit your system, and in addition you need the build folder of your ROOT install.

Appendix G

Other appendices

Kinematics in the lab frame for ^{140}Sm on ^{208}Po at 4.65 MeV/u



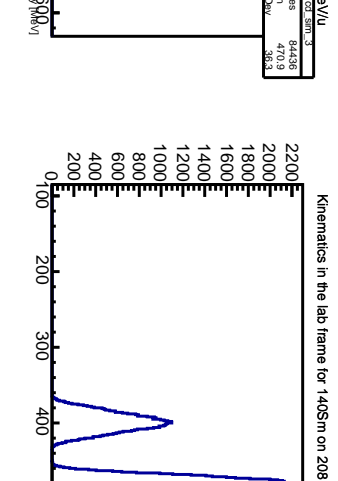
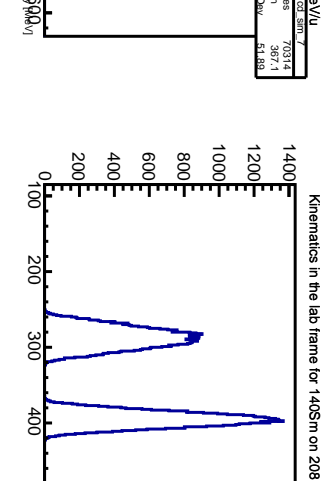
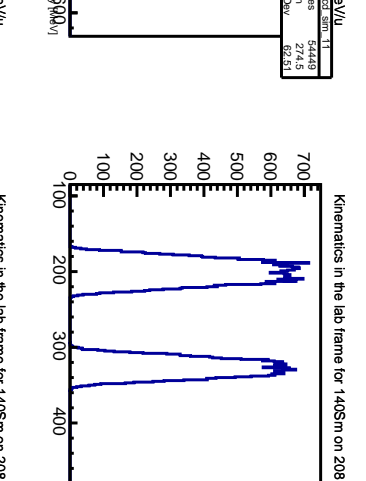
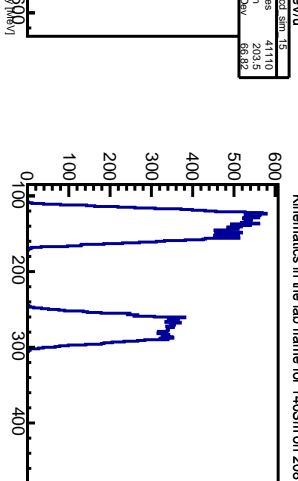
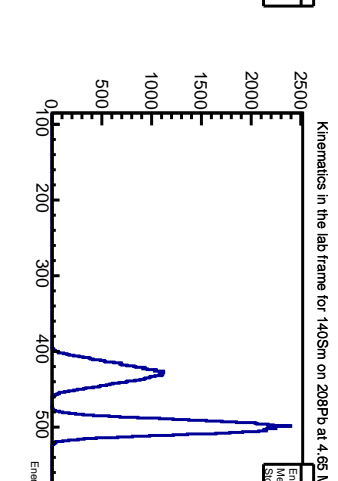
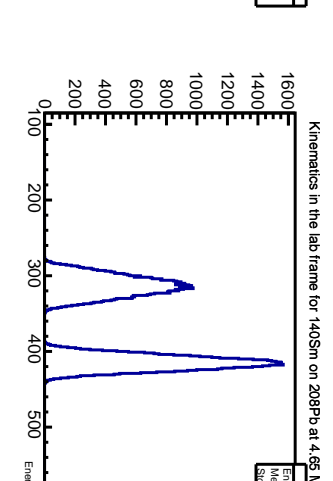
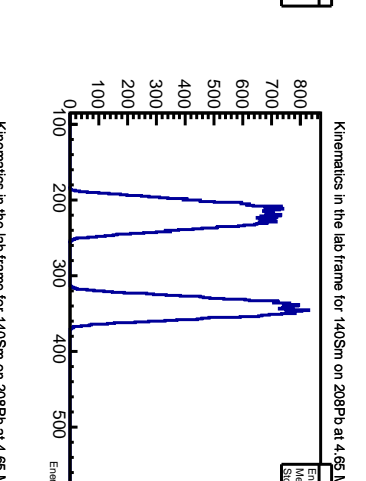
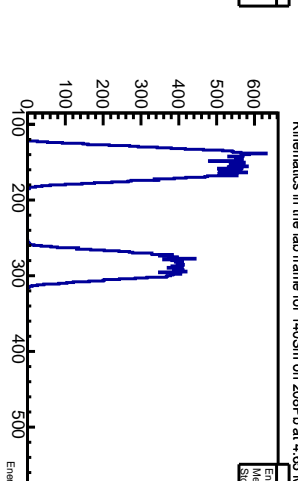
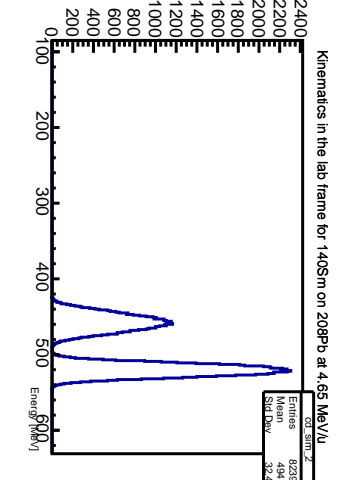
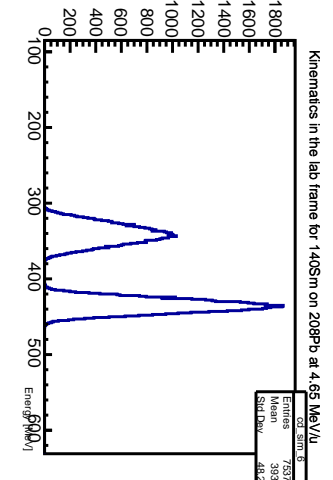
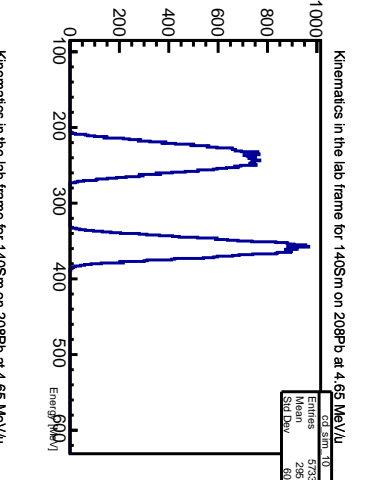
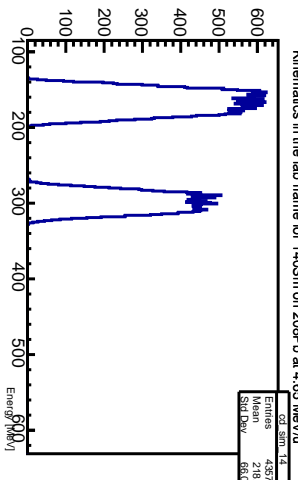
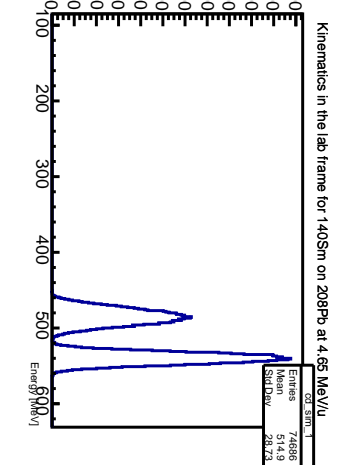
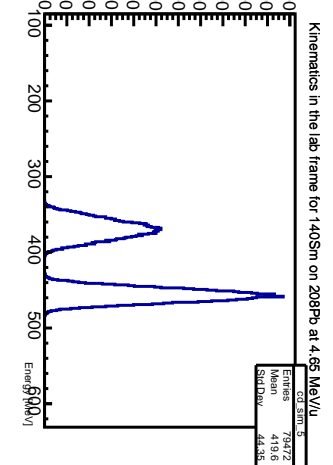
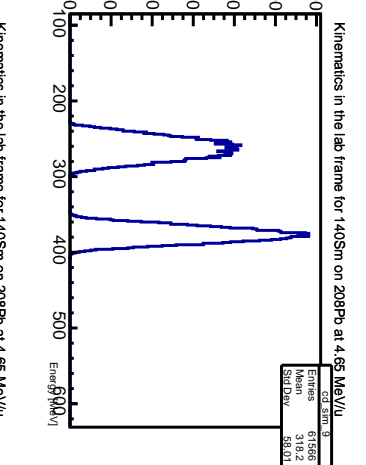
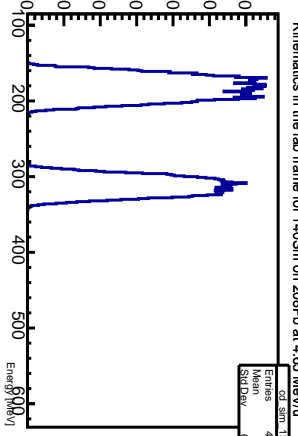
Kinematics in the lab frame for ^{140}Sm on ^{208}Po at 4.65 MeV/u



Kinematics in the lab frame for ^{140}Sm on ^{208}Po at 4.65 MeV/u



Kinematics in the lab frame for ^{140}Sm on ^{208}Po at 4.65 MeV/u



Bibliography

- [1] M. Klintefjord. *Evolution of deformation and collectivity away from magic numbers*. PhD thesis, University of Oslo, May 2016. URL <http://urn.nb.no/URN:NBN:no-56121>.
- [2] M. Klintefjord, K. Hadyńska-Klęk, J. Samorajczyk, et al. Spectroscopy of low-lying states in ^{140}Sm . *Acta Physica Polonica B*, 46(3):607–611, 2015. ISSN 0587-4254. doi: 10.5506/APhysPolB.46.607.
- [3] J. Samorajczyk, M. Klintefjord, C. Droste, et al. Revised spin values of the 991 keV and 1599 keV levels in Sm 140. *Physical Review C - Nuclear Physics*, 92(4):3–6, 2015. ISSN 1089490X. doi: 10.1103/PhysRevC.92.044322.
- [4] M. Klintefjord, K. Hadyńska-Klęk, A. Görzen, et al. Structure of low-lying states in Sm 140 studied by Coulomb excitation. *Physical Review C*, 93(5): 1–14, 2016. ISSN 24699993. doi: 10.1103/PhysRevC.93.054303.
- [5] NIST Physics Laboratory web site. URL <https://physics.nist.gov/constants>. Accessed: July 2019.
- [6] P. Reiter, J. Eberth, H. Faust, et al. The MINIBALL array. *Nuclear Physics A*, 701(1-4):209–212, 2002. ISSN 03759474. doi: 10.1016/S0375-9474(01)01576-7.
- [7] M. J. Borge and K. Riisager. HIE-ISOLDE, the project and the physics opportunities. *European Physical Journal A*, 52(11), 2016. ISSN 1434601X. doi: 10.1140/epja/i2016-16334-4.
- [8] The ISOLDE web page. URL <http://isolde.web.cern.ch>. Accessed: July 2019.
- [9] B. Jonson and K. Riisager. The ISOLDE facility. *Scholarpedia*, 5(7):9742, 2010. doi: 10.4249/scholarpedia.9742. Revision #90796.
- [10] Nucleonica Newsletter, 2019. URL <https://www.nucleonica.com/wiki/images/c/cb/NucleonicaNewsletter2019.pdf>. Accessed: July 2019.

- [11] D. Olsen. First generation ISOL radioactive ion beam facilities. pages 312–316, 2002. doi: 10.1109/pac.1995.504646.
- [12] N. Warr, J. Van de Walle, M. Albers, et al. The miniball spectrometer. *European Physical Journal A*, 49(3):1–32, 2013. ISSN 1434601X. doi: 10.1140/epja/i2013-13040-9.
- [13] C. Lefèvre. The CERN accelerator complex. Complexe des accélérateurs du CERN. Dec 2008. URL <https://cds.cern.ch/record/1260465>.
- [14] R. Catherall, W. Andreazza, M. Breitenfeldt, et al. The ISOLDE facility. 2, 2017. ISSN 13616471. doi: 10.1088/1361-6471/aa7eba.
- [15] M. J. Borge. The ISOLDE facility: Recent highlights and the HIE-ISOLDE project. *Proceedings of Science*, 11005:1–8, 2013. ISSN 18248039.
- [16] The ISOLDE RILIS web page. URL <http://rilis.web.cern.ch>. Accessed: July 2019.
- [17] B. A. Marsh, B. Andel, A. N. Andreyev, et al. New developments of the in-source spectroscopy method at RILIS/ISOLDE. *Nuclear Instruments and Methods in Physics Research, Section B: Beam Interactions with Materials and Atoms*, 317(PART B):550–556, 2013. ISSN 0168583X. doi: 10.1016/j.nimb.2013.07.070. URL <http://dx.doi.org/10.1016/j.nimb.2013.07.070>.
- [18] T. D. Goodacre, V. Fedossev, S. Rothe, et al. Ion beam production and study of radioactive isotopes with the laser ion source at ISOLDE. *Journal of Physics G: Nuclear and Particle Physics*, 44(8):084006, 2017. ISSN 0954-3899. doi: 10.1088/1361-6471/aa78e0.
- [19] E. Kugler, D. Fiander, B. Johnson, et al. The new CERN-ISOLDE on-line mass-separator facility at the PS-Booster. *Nuclear Inst. and Methods in Physics Research, B*, 70(1-4):41–49, 1992. ISSN 0168583X. doi: 10.1016/0168-583X(92)95907-9.
- [20] P. Schmidt, F. Ames, G. Bollen, et al. Bunching and cooling of radioactive ions with REXTRAP. *Nuclear Physics A*, 701(1-4):550–556, 2002. ISSN 03759474. doi: 10.1016/S0375-9474(01)01642-6.
- [21] F. Ames, G. Bollen, P. Delahaye, et al. Cooling of radioactive ions with the Penning trap REXTRAP. *Nuclear Instruments and Methods in Physics Research, Section A: Accelerators, Spectrometers, Detectors and Associated Equipment*, 538(1-3):17–32, 2005. ISSN 01689002. doi: 10.1016/j.nima.2004.08.119.

- [22] B. H. Wolf, J. Cederkäll, O. Forstner, et al. First radioactive ions charge bred in REXEBIS at the REX-ISOLDE accelerator. *Nuclear Instruments and Methods in Physics Research, Section B: Beam Interactions with Materials and Atoms*, 204:428–432, 2003. ISSN 0168583X. doi: 10.1016/S0168-583X(02)02108-0.
- [23] Y. Kadi, Y. Blumenfeld, W. V. Delsolaro, et al. Post-accelerated beams at ISOLDE. *Journal of Physics G: Nuclear and Particle Physics*, 44(8), 2017. ISSN 13616471. doi: 10.1088/1361-6471/aa78ca.
- [24] The REX-ISOLDE web page. URL <http://rex-isolde.web.cern.ch>. Accessed: July 2019.
- [25] The HIE-ISOLDE web page. URL <http://hie-isolde-project.web.cern.ch>. Accessed: July 2019.
- [26] F. Wenander. EBIS as charge breeder for radioactive ion beam accelerators. *Nuclear Physics A*, 701(1-4):528–536, 2002. ISSN 03759474. doi: 10.1016/S0375-9474(01)01640-2.
- [27] F. Wenander. Charge breeding of radioactive ions with EBIS and EBIT. *Journal of Instrumentation*, 5(10), 2010. ISSN 17480221. doi: 10.1088/1748-0221/5/10/C10004.
- [28] F. L. Bello Garrote, A. Görgen, J. Mierzejewski, et al. Lifetime measurement for the 21+ state in Sm 140 and the onset of collectivity in neutron-deficient Sm isotopes. *Physical Review C - Nuclear Physics*, 92(2):1–8, 2015. ISSN 1089490X. doi: 10.1103/PhysRevC.92.024317.
- [29] N. Warr. *The Miniball double-sided silicon strip detector (CD)*, October 2015. URL <https://www.ikp.uni-koeln.de/~warr/doc/cd.pdf>. Accessed: April 2019.
- [30] A. N. Ostrowski, S. Cherubini, T. Davinson, et al. CD: A double sided silicon strip detector for radioactive nuclear beam experiments. *Nuclear Instruments and Methods in Physics Research, Section A: Accelerators, Spectrometers, Detectors and Associated Equipment*, 480(2-3):448–455, 2002. ISSN 01689002. doi: 10.1016/S0168-9002(01)00954-8.
- [31] N. Warr. *The Miniball Cluster*, March 2005. URL https://www.ikp.uni-koeln.de/~warr/doc/miniball_detectors.pdf. Accessed: July 2019.
- [32] P. A. Butler, J. Cederkall, and P. Reiter. Nuclear-structure studies of exotic nuclei with MINIBALL. *Journal of Physics G: Nuclear and Particle Physics*, 44(4), 2017. ISSN 1361-6471. doi: 10.1088/1361-6471/aa5c4e.

- [33] N. Warr. *Miniball Flexible Frame*, March 2015. URL <https://www.ikp.uni-koeln.de/~warr/doc/frame.pdf>. Accessed: July 2019.
- [34] R. Lutter, O. Schaile, K. Schoffel, et al. MARaBOOU-A MBS and ROOT based online/offline utility. *SANTA FE 1999 - 11th IEEE NPSS Real Time Conference, Conference Record, RT 1999*, (May):363–366, 1999. doi: 10.1109/RTCON.1999.842643.
- [35] H. G. Essel and N. Kurz. The general purpose data acquisition system MBS. *SANTA FE 1999 - 11th IEEE NPSS Real Time Conference, Conference Record, RT 1999*, 41(2):475–478, 1999. doi: 10.1109/RTCON.1999.842672.
- [36] R. Brun and F. Rademakers. ROOT - An Object Oriented Data Analysis Framework. Proceedings AIHENP'96 Workshop, Lausanne, Sep. 1996, Nucl. Inst. & Meth. in Phys. Res. A 389 (1997) 81-86. URL <https://github.com/root-project/root>. doi: 10.5281/zenodo.2557526. Download: December 2018.
- [37] L. Gaffney. Kinematics simulations for Coulomb-excitation experiments at Miniball. URL <https://github.com/lpgaff/kinsim>. Download: May 2018.
- [38] The Stopping and Range of Ions in Matter. URL <http://www.srim.org>. Download: February 2018.
- [39] Analysis code for MINIBALL experiments at ISOLDE. URL <https://github.com/Miniball/MiniballCoulexSort>. doi: 10.5281/zenodo.2593370. Download: March 2019.